

FERROMAGNETISM IN (Ga,Mn)As AND (Ga,Mn)N

HANNES RAEBIGER

Laboratory of Physics
Helsinki University of Technology
Espoo, Finland

Dissertation for the degree of Doctor of Science in Technology to be presented with due permission of the Department of Engineering Physics and Mathematics for public examination and debate in Auditorium E at Helsinki University of Technology (Espoo, Finland) on the 21st of April, 2006, at 12 o'clock noon.

*Dissertations of Laboratory of Physics,
Helsinki University of Technology
ISSN 1455-1802*

*Dissertation 139 (2006):
Hannes Raebiger: Ferromagnetism in (Ga,Mn)As and (Ga,Mn)N
ISBN 951-22-8121-X (print)
ISBN 951-22-8122-8 (electronic)
URL <http://lib.tkk.fi/Diss/2006/isbn9512281228>*

Picaset Oy
Helsinki 2006

He who controls magnetism controls the universe!

—Diet Smith¹

¹Inventor of Dick Tracy's Space Coupe in the Comics by Chester Gould

Tiivistelmä

(Ga,Mn)As ja (Ga,Mn)N ovat magneettisia puolijohdeita, joita voidaan valmistaa vastaavista yhdistepuolijohdeista seostamalla niitä sopivalla magneettisella alkuaineella kuten mangaanilla. Nämä materiaalit ovat luonnostaan hyvä vaihtoehto elektroniikkakomponenttien hankalille metalli-puolijohde -rajapinnoille. Ne soveltuvat myös sellaisenaan nk. spintroniikka-sovelluksiin, joissa hyödynnetään samanaikaisesti elektronin varausta ja spin-tilaa. Ensin on kuitenkin ymmärrettävä magnetismiin johtavat fysikaaliset mekanismit, jotta voisimme suunnitella uusia magneettisia puolijohdemateriaaleja tai kehittää sovelluksia olemassaoleville. Tässä väitöskirjassa esitän teoreettisen tutkimuksen kahden tärkeimmän prototyypimateriaalin — (Ga,Mn)As ja (Ga,Mn)N — rakenteellisista ja magneettisista ominaisuuksista.

Ferromagnetismi pohjautuu kvanttimekaaniselle vaihtovuorovaikutukselle, mutta on luonteeltaan makroskooppinen järjestäytymisilmiö. Ferromagneetteja täytyykin tarkastella eri mitta-asteikoilla lähtien kvanttimekaniikasta. Niin mikroskooppisten rakenteiden energiat kuin niihin liittyvät magneettiset vuorovaikutuksetkin lasketaan *ab initio*-menetelmällä. Näitä energioita käytetään Monte Carlo -simulaatioissa, joilla tutkitaan makroskooppisia ja äärellisen lämpötilan ominaisuuksia. Curie -lämpötilat lasketaan sekä Weissin molekyylikenttäteorialla että Monte Carlo -simulaatioilla.

Näytän tässä väitöskirjatyössä, että tarkastellut prototyypimateriaalit (Ga,Mn)As ja (Ga,Mn)N rakentuvat oleellisesti mangaaniklustereista, ja nämä klusterit ovat elektronisilta ja magneettisilta ominaisuuksiltaan hyvin erilaisia kuin yksittäiset mangaaniatomit. (Ga,Mn)As:lle esitän myös vakanssidiffuusiomekanismin, joka kineettisten Monte Carlo -simulaatioiden mukaan johtaa klusterointiin tyypillisissä kiteenkasvatus- ja toivutusolosuhteissa. Klusterointi alentaa kummankin materiaalin Curie -lämpötiloja, joskin alenemisen aiheuttava vyörakenteen kehitys on erilaista. (Ga,Mn)As:n Curie -lämpötila arvioidaan Weissin molekyylikenttäteoriasta, mutta (Ga,Mn)N:lle käytetään tarkempaa Monte Carlo -menetelmää.

Abstract

(Ga,Mn)As and (Ga,Mn)N are so called diluted magnetic semiconductors, i.e. semiconductor based materials made ferromagnetic by inclusion of a magnetic element—in this case Mn. This type of materials bridge over the incompatibilities in metal–semiconductor interfaces in electronics components and have an enormous potential for future spintronics applications, where both charge and spin degrees of freedom can be employed simultaneously. In order to design new—or employ the existing—diluted magnetic semiconductor materials, the underlying mechanisms of magnetism must be understood. In this work a theoretical study of the structural and magnetic properties of the two most important prototype materials, (Ga,Mn)As and (Ga,Mn)N, is presented.

Ferromagnetism arises from the quantum mechanical exchange interactions, but is by its very nature a macroscopic ordering effect. Therefore a multiscale approach is employed, beginning from quantum mechanical interactions. Both microscopic configurational energies and corresponding magnetic interactions are calculated from first principles. These energies are used in Monte Carlo simulations to study macroscopic and finite temperature properties. Curie temperatures are estimated using the Weiss molecular field theory, as well as a more sophisticated Monte Carlo approach.

We show that both (Ga,Mn)As and (Ga,Mn)N consist largely of Mn clusters, and that the electronic and magnetic properties of these clusters differ significantly from those of single substitutional impurities. For (Ga,Mn)As we also show using lattice kinetic Monte Carlo methods that clustering occurs during growth and annealing via the Ga monovacancy mediated diffusion. For both materials clustering efficiently reduces the Curie temperatures even though the underlying band structure trends are different. The Curie temperatures are estimated for (Ga,Mn)As using the Weiss molecular field theory, while for (Ga,Mn)N we employ Monte Carlo methods in order to obtain the Curie temperatures.

Preface

The work reported in this Thesis was carried out at the Laboratory of Physics COMP group at Helsinki University of Technology. I am grateful to Academy Professor Risto Nieminen for giving me the opportunity to pursue doctoral studies in the COMP group, for suggesting the topic, and for providing me with all the necessary facilities. I am indebted to Professor Juhani von Boehm for supervising this work; his patience and wise guidance has helped me focus on the essential, i.e. understanding fundamental physics. I also wish to thank Dr. Andrés Ayuela, who has been mentoring me since 1999, even over long distance in the past few years. Besides sharing his overwhelming knowledge on magnetism, Andrés has become a dear friend to me.

I am grateful for Mr. Teemu Hynninen (MSc) for vitalizing our magnetism group with his fresh ideas and great mathematical talent. Teemu made an invaluable contribution to the last stages of this work. I also thank Dr. Maria Ganchenkova for her important contribution. I am indebted to Prof. Kimmo Saarinen for the many inspiring discussions—Kimmo’s too early departure left an unfillable vacancy in our laboratory and the entire semiconductor physics community. My gratitude goes also to Drs Filip Tuomisto and Petteri Pusa for sharing their unpublished experimental diffusion results. Thanks for all the scientific and non-scientific discussions with the lot of you at the Lab of Physics.

I am grateful for the generous CPU resources from the Center for Scientific Computing CSC, the financial support from the Finnish Cultural Fund, and the Scandinavia-Japan Sasakawa Foundation for several travel grants.

Most importantly, I thank Yoko for standing beside me these few, long years. Thank you for singing like an angel, reminding me of what is important in life.

Otaniemi, February 2006
Hannes Raebiger

Table of Contents

List of publications	ix
1 Introduction	1
1.1 III-V based materials	3
1.2 (Ga,Mn)As	4
1.3 (Ga,Mn)N	5
2 Theoretical modeling	7
2.1 Temperature dependence of ferromagnetism	7
2.1.1 Effects of inhomogeneities	10
2.2 Density-functional theory	11
2.2.1 XC functionals	13
2.2.2 The projector augmented-wave method	14
2.2.3 Total energy calculations	16
3 (Ga,Mn)As	17
3.1 Microscopic structure	17
3.1.1 Kinetic considerations	19
3.2 Band structure	23
3.3 Curie temperature	25
4 (Ga,Mn)N	29
4.1 Microscopic structure	29
4.2 Band structure and magnetic properties	31
4.2.1 Molecular field theory	31
4.2.2 Monte Carlo simulations	33

5	Summary and outlook	37
5.1	(Ga,Mn)As	38
5.2	(Ga,Mn)N	38

List of publications

This Thesis consists of an overview and the following publications:

- I. H. Raebiger, A. Ayuela, and R. M. Nieminen,
“*Intrinsic hole localization in magnetic semiconductors,*”
Journal of Physics: Condensed Matter **16**, L457–L462 (2004).
©2004 IOP Publishing Ltd. By permission.
- II. H. Raebiger, A. Ayuela, J. von Boehm, and R. M. Nieminen,
“*Clustering of Mn in (Ga,Mn)As,*”
Journal of Magnetism and Magnetic Materials **290-291**, 1398–
1401 (2005). ©2005 Elsevier. By permission.
- III. H. Raebiger, T. Hynninen, A. Ayuela, and J. von Boehm,
“*The effects of clustering on ferromagnetism in (Ga,Mn)As,*”
Physica B (in press) (4 pages). ©2005 Elsevier. By permission.
- IV. H. Raebiger, A. Ayuela, and J. von Boehm,
“*Electronic and magnetic properties of substitutional Mn clusters
in (Ga,Mn)As,*”
Physical Review B **72**, 014465 (2005) (7 pages). ©2005 The
American Physical Society. By permission.
- V. H. Raebiger, M. G. Ganchenkova, and J. von Boehm,
“*Diffusion and clustering of substitutional Mn in (Ga,Mn)As,*”
cond-mat/0603135 (2006) (4 pages).
- VI. T. Hynninen, H. Raebiger, A. Ayuela, and J. von Boehm,
“*High Curie temperatures in (Ga,Mn)N from Mn clustering,*”
Applied Physics Letters **88**, 122501 (2006) (3 pages). ©2006
American Institute of Physics. By permission.
- VII. T. Hynninen, H. Raebiger, and J. von Boehm,
“*A multiscale study of ferromagnetism in clustered (Ga,Mn)N,*”
Journal of Physics: Condensed Matter **18**, 1561–1567 (2006).
©2006 IOP Publishing Ltd. By permission.

The author has had an active role in all phases of the research reported in this Thesis. He has had the main responsibility of planning the calculations and interpreting the results. All calculations presented in Publications I–V were carried out by the author, except for the FLAPW test calculation in Publication I and the kinetic Monte Carlo calculations in Publication V, which were carried out by Dr. Andrés Ayuela and Dr. Maria Ganchenkova, respectively. The calculations in Publications VI and VII were carried out by Mr. Teemu Hynninen (MSc) under the author’s supervision. The author has had an important role in the development of the statistical model presented in Publication VII. Publications III and V were wholly written by the author, and in Publications I, II, IV, VI, VII the author has been the corresponding author and has had central responsibility in the writing.

CHAPTER 1

Introduction

Conventional, nonmagnetic semiconductors can be made magnetic by inclusion of transition metal atoms in the semiconductor lattice. The first material of this kind was (In,Mn)As [1], where Mn atoms substitutionally replace In atoms in the InAs semiconductor. Ferromagnetic semiconductors would be the natural choice to overcome material incompatibilities in metal-semiconductor interfaces, and exhibit a plethora of new possibilities to intertwine magnetic properties with existing semiconductor technologies [2, 3]. The enormous potential of this type of materials was immediately recognized, which initiated the ongoing quest for a fully-fledged room temperature magnetic semiconductor material that is compatible with existing semiconductor technologies. Numerous new magnetic materials have been discovered or proposed, mostly based on III-V and II-VI compound semiconductors with embedded Cr, Mn or Co atoms. These materials are usually referred to as diluted magnetic semiconductors.

Theoretical understanding of basic material properties is crucial before actual applications can be designed. In diluted magnetic semiconductors, the key task lies in unveiling the origin of ferromagnetic ordering. Magnetic atoms are introduced into a typically nonmagnetic host material, and one needs to understand what is the coupling mechanism between these magnetic atoms and why they align ferromagnetically. More practically, what is the critical temperature where ferromagnetic order disappears (i.e. Curie temperature T_C). More importantly, for what materials is the Curie temperature above room temperature. The basic magnetic properties may be described in terms of phenomenological models [4, 5], which however include a number of ambiguous parameters, and it is not obvious when and where the models are

1. Introduction

applicable. Nevertheless, the microscopic interactions are directly accessible via quantum mechanical first principles, i.e. parameter free calculations, but alas, the description of the physical properties of macroscopic bodies based solely on the microscopic properties is not possible and some approximations must be made.

There has been a tremendous theoretical effort to understand the basic properties of the diluted magnetic semiconductor materials [4–7], especially based on first principles calculations [8–19]. In spite of these efforts a number of open questions remain. It turns out that in some of these diluted magnetic semiconductors the ferromagnetism is carrier mediated, i.e. magnetic properties can be tuned by charge carrier manipulation, while in other materials the mechanism of magnetism may be different. Predicting the Curie temperature, whether it is related to carrier mediated ferromagnetism or some other mechanism remains one of the main tasks.

A key aspect in understanding the magnetism of diluted magnetic semiconductors lies in understanding their magnetic structures at different length scales. Large scale disorder effects in the dilute limit have a tendency to increase the Curie temperature [20–23], while at large concentration of the magnetic atoms (i.e. in the atomic percent regime) the effect is opposite [17, 23–27]. The relevance of large scale disorder effects and percolation depends also on whether the microscopic interactions are of long or short range [16, 18, 24, 26], and whether the microscopic interactions on the other hand depend on the microscopic (cluster) structure [28–30]. The main objective of this thesis work is to find a way to combine these different length scale effects in the study of magnetic properties of diluted magnetic semiconductors.

In this Thesis we focus on two prototype III-V diluted magnetic semiconductor materials (Ga,Mn)As and (Ga,Mn)N. Although these materials exhibit quite different properties from one another, their microscopic structures are closely related. We find, common for both these materials that the Mn atoms have a tendency to form clusters around the As or N atom. We take this microscopic clustering into account and estimate the Curie temperatures for (Ga,Mn)As and (Ga,Mn)N.

§1.1. III-V based materials

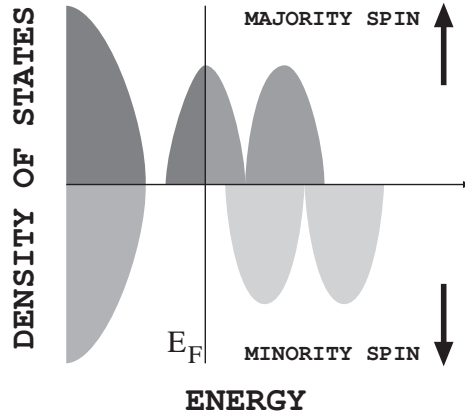


Figure 1.1. Typical density of states for a half-metal.

§1.1 III-V based materials

Soon after the discovery of (In,Mn)As [1], similar materials have been prepared by introducing Mn¹ atoms into a III-V compound semiconductor. The diluted magnetic semiconductor no longer exhibits the typical band structure of a semiconductor, as one of the spin components has a partially filled band, while the other one is fully occupied. This kind of materials are called half-metals [31, 32], and a typical band structure of a half-metal is given in Figure 1.1. The half-metals are thus metallic for one spin component, and insulating (or semiconducting) for the other one. This leads to the interesting property that half-metals are fully spin polarized: all charge carriers have the same spin. Furthermore, half-metals have a “quantized” magnetic moment M . As the bands of the non-conducting spin component are fully occupied, the occupation number of electrons per unit cell with that spin (\downarrow in Fig. 1.1) must be an integer N^\downarrow , and consequently also the metallic bands get an integer occupation number ($N^\uparrow = N - N^\downarrow$, where N is total number of electrons per unit cell). Thus also the magnetic moment $M = (N^\uparrow - N^\downarrow)\mu_B$ has an integer value of Bohr magnetons μ_B . In normal magnetic metals both N^\downarrow and N^\uparrow are partially occupied

¹Also other transition metals have been applied, as well as rare earths such as Gd.

1. Introduction

and neither of them is necessarily an integer (e.g. for iron the magnetic moment per atom is $2.2 \mu_B$).

The most important and most widely studied prototype materials of the III-V diluted magnetic semiconductor family are (Ga,Mn)As and (Ga,Mn)N. Both of these materials have rather high Curie temperatures [33–35], but the electronic properties, and possibly also the origin of magnetism, are quite different.

§1.2 (Ga,Mn)As

(Ga,Mn)As has been widely studied [36–38], because of its rather high Curie temperature (T_C) of up to 170 K [33, 34]. The ferromagnetic coupling is generally believed to be mediated by the holes that are created by the Mn atoms when they substitute Ga atoms. In principle, each substitutional Mn atom (Mn_{Ga}) should induce one hole. However, the hole concentrations observed in the experimental samples are only a fraction of the expected (0.03–0.3 of the Mn concentration $[\text{Mn}]$) [39].

The material is usually grown epitaxially at low temperatures and the as-grown samples typically exhibit $T_C \lesssim 110$ K. The epitaxial growth leads also to the formation of As antisites (As_{Ga}) and interstitial Mn (Mn_i), which act as donors, thus compensating Mn_{Ga} induced holes. This hole compensation also hampers the hole mediated ferromagnetism. Post-growth annealing at temperatures close to the growth temperature leads to out-diffusion of the undesired Mn_i , thus increasing T_C up to 170 K [33, 34]. However, T_C exhibits twofold behavior with respect to the annealing time: (1) annealing for a few hours increases T_C due to the out-diffusion of Mn_i , while (2) prolonged annealing for ten hours or longer reduces T_C again. [40–42] The mechanism behind the long-term lowering of T_C is not known.

The band structure and magnetic properties of a single substitutional Mn are rather wellknown [14, 19, 43–47], but effects due to inhomogeneous Mn substitution and consequential Mn clustering lack comprehensive understanding. This is also reflected to the Curie temperature, as first principles calculations usually predict significantly larger T_C values [14–19, 25] than experimentally observed. These inhomogeneity induced effects are explored in Publications I–V, and summarized in Chapter 3.

§1.3 (Ga,Mn)N

The growth of $(Ga,Mn)N$ is not as well controlled as that of $(Ga,Mn)As$ (see e.g. [35]). Second phase formation is difficult to avoid [48, 49], which is also reflected in the lack of theoretical understanding of this material. The mechanisms underlying ferromagnetism are not understood, and there is no clear consensus of what is the microscopic structure of $(Ga,Mn)N$.

The magnetic interactions between individual substitutional Mn atoms are widely studied, and known to have shorter range than those in $(Ga,Mn)As$ [16–18, 25]. However, the effects of inhomogenities in Mn substitution need to be investigated in detail. Contrary to $(Ga,Mn)As$, the Curie temperature of $(Ga,Mn)N$ is not even experimentally well established, as measured values range from close to zero Kelvin to 940 K [49–56]. Especially the high T_C values observed experimentally lack theoretical understanding. The inhomogeneity effects as well as related fluctuations in T_C calculated within different approximations are investigated in Publications VI and VII, and summarized in Chapter 4.

Theoretical modeling

Paramagnetic materials exhibit a macroscopic magnetization \vec{M} parallel to an external field \vec{B} , which vanishes in the absence of \vec{B} . The magnitude and temperature dependence of \vec{M} were already described in 1905 by Langevin [57]. Ferromagnetic materials are the ones commonly known as magnets, where a non-vanishing magnetization remains even in the absence of an external field.

In this chapter the temperature dependence of ferromagnetism is described using the Weiss molecular field theory [58] combined with a quantum mechanical description for the molecular field based on the model suggested by Heisenberg [59]. To calculate these quantum mechanical interactions the density-functional theory [60] together with the projector augmented-wave method [61, 62] are introduced. We also present a Monte Carlo scheme based on the calculated quantum mechanical interactions which improves the evaluation of the finite temperature magnetic properties of diluted magnetic semiconductors.

§2.1 Temperature dependence of ferromagnetism

Assume that a ferromagnetic material consists of magnetic particles with magnetic moment $\vec{\mu}$. The magnetic moments are aligned parallel at low temperatures, exhibiting the magnetization $\vec{M} = N\vec{\mu}$, where N is the number of magnetic particles per unit volume. Weiss postulated that this alignment is due to an internal field—the molecular field \vec{B}_{mol} —that is (i) parallel to the magnetization, i.e. $\vec{B}_{\text{mol}} \uparrow\uparrow \vec{M}$; and (ii)

2. Theoretical modeling

proportional to the magnetization, i.e. $\vec{B}_{\text{mol}} = a\mu_0\vec{M} = a\mu_0N\vec{\mu}$ [58]. μ_0 is the vacuum permeability and a a constant to be determined. For paramagnetic materials, the magnetization \vec{M} is proportional to the external field \vec{B} , but in the case of ferromagnetic materials \vec{B} must be replaced by the sum $\vec{B}' = \vec{B} + \vec{B}_{\text{mol}} = \vec{B} + aN\mu_0\vec{\mu}$.

Quantum mechanically we may identify the single magnetic moments as those of atoms, determined by their spin quantum number S and having the magnitude $-Sg\mu_B$ in the chosen direction, where g is the Landé factor and μ_B the Bohr magneton. The Curie temperature T_C based on the Weiss molecular field theory can be written as [63, 64]

$$T_C = \frac{Na\mu_0S(S+1)(g\mu_B)^2}{3k_B}. \quad (2.1)$$

It is easy to deduce from experimental Curie temperatures what values the inner field \vec{B}_{mol} should have. The origin of \vec{B}_{mol} remained unknown until Heisenberg suggested that the internal field is due to the quantum mechanical exchange interactions [59]. In the Heisenberg model, the Hamiltonian of a ferromagnet may be written as

$$H = - \sum_{i,j} J_{ij} \vec{s}_i \cdot \vec{s}_j = -2 \sum_{(i,j)} J_{ij} \vec{s}_i \cdot \vec{s}_j, \quad (2.2)$$

where \vec{s}_i denote the individual spins and J_{ij} is the exchange integral [59]. Notice that $J_{ii} \equiv 0$, $\sum_{i,j}$ and $\sum_{(i,j)}$ denote a double sum and a sum over all pairs, respectively. The interaction energy operator of atoms i and j with localized orbitals—assuming that the interatomic exchange integrals only depend on internuclear distance, and that intra-atomic exchange leads to the same total energy irrespective of the atom's angular momentum—can be expressed as [63]

$$-2J_{ij} \left(\sum_k^{\text{atom } i} \vec{s}_k \right) \cdot \left(\sum_l^{\text{atom } j} \vec{s}_l \right) = -2J_{ij} \vec{S}_i \cdot \vec{S}_j \quad (2.3)$$

$$\implies H = - \sum_{i,j} J_{ij} \vec{S}_i \cdot \vec{S}_j = -2 \sum_{(i,j)} J_{ij} \vec{S}_i \cdot \vec{S}_j. \quad (2.4)$$

Here \vec{S}_i is the vector sum of spins \vec{s}_k belonging to the i th atom. The energy operator of atom 0 with magnetic moment $-g\mu_B\vec{S}_0$ in the inner magnetic field \vec{B}_{mol} is $g\mu_B\vec{S}_0 \cdot \vec{B}_{\text{mol}}$, and on the other hand according

§2.1. *Temperature dependence of ferromagnetism*

to Eq. (2.3) this should equal $-2\vec{S}_0 \cdot \sum_i J_{i0}\vec{S}_i$, which describes the interaction energy of the 0th atom with all other atoms in the system. Thus the Weiss inner field operator and its expectation value read

$$\vec{B}_{\text{mol}} = \frac{-2 \sum_i J_{i0} \vec{S}_i}{g\mu_B}, \quad \langle \vec{B}_{\text{mol}} \rangle = \frac{-2 (\sum_i J_{i0}) \langle \vec{S} \rangle}{g\mu_B}, \quad (2.5)$$

where $\langle \vec{S} \rangle$ is the average spin per atom, which corresponds to the magnetic moment $-\langle \vec{S} \rangle g\mu_B$. On the other hand, the average magnetic moment per atom in unit volume is \vec{M}/N , yielding the inner field expectation value

$$\langle \vec{B}_{\text{mol}} \rangle = \frac{2 \sum_i J_{i0} \vec{M}}{(g\mu_B)^2 N} = a\mu_0 \vec{M}. \quad (2.6)$$

The above expression identifies the coefficient $a\mu_0$ that gives the inner field magnitude, and substituting to Eq. (2.1) yields

$$T_C = \frac{2 \sum_i J_{i0}}{3k_B} S(S+1). \quad (2.7)$$

In order to predict Curie temperatures, one has to estimate the magnitude of the exchange field, or more precisely the sum of exchange integrals $\sum_i J_{i0}$. In general, it cannot be solved exactly, but to rather good approximation from state-of-the-art total energy calculations as outlined below. The total energy E^{tot} consists of a term from the Heisenberg Hamiltonian and some other terms, i.e. $E^{\text{tot}} = E_0 - \langle \sum_{i,j} J_{ij} \vec{S}_i \cdot \vec{S}_j \rangle$. Assuming that E_0 is constant, the total energy difference per atom Δ between a system in antiferromagnetic E^{A} and ferromagnetic E^{F} states is approximately

$$\Delta = \frac{1}{N} (E^{\text{A}} - E^{\text{F}}) = \frac{1}{N} \left\langle \sum_{i,j} J_{ij} \vec{S}_i \cdot \vec{S}_j \right\rangle = S^2 \sum_i J_{i0}, \quad (2.8)$$

because the Heisenbergian term for an antiferromagnetic state is approximately zero, and the product of spins \vec{S}_i and \vec{S}_j yields an expectation value of S^2 [65]. Substituting this into Eq. (2.7) gives

$$T_C = \frac{2\Delta}{3k_B} \frac{S(S+1)}{S^2} \approx \frac{2\Delta}{3k_B}. \quad (2.9)$$

2. Theoretical modeling

The approximation holds for large S . Now the Curie temperature is easily accessed through total energy calculations that will be described in §2.2. Virtually the same equation has also been presented in Refs [29, 30, 46, 66–69]. In the coherent-potential approximation usually the local moment disorder state is considered as the reference instead of the antiferromagnetic state—either one may be used as their total energies are nearly the same [68].

§2.1.1 Effects of inhomogeneities

The above mean field description tends to overestimate Curie temperatures, because actual samples are never completely homogeneous, and therefore neither the inner field is necessarily homogeneous.¹ Spins may locally form clusters that have a strong internal field, while the inner field between such clusters may be weaker. One way to go about this is to regroup the Heisenberg Hamiltonian as

$$H = - \sum_{i,j} J_{ij} \left(\sum_{k \text{ cluster } i} \vec{s}_k \right) \cdot \left(\sum_{l \text{ cluster } j} \vec{s}_l \right) = - \sum_{i,j} J_{ij} \vec{S}_i \cdot \vec{S}_j, \quad (2.10)$$

instead of expression (2.4). Now \vec{S}_i represents the cluster spin instead of that of a single atom, but the Curie temperature may be estimated exactly in the same manner as above using Eq. (2.9) and simply replacing the atoms with clusters.

This expression neglects the internal magnetic structure of the clusters, and thus still may exaggerate Curie temperatures. In particular for large clusters, the assumption that intra-cluster exchange may be neglected not necessarily holds. Therefore a term E_i , which describes the internal energy of the i th cluster is added, yielding the modified Hamiltonian

$$H' = - \sum_{i,j} J_{ij} \vec{S}_i \cdot \vec{S}_j - \sum_i E_i. \quad (2.11)$$

Due to the E_i term however, T_C is no longer directly accessible with simple expressions like Eq. (2.9). It becomes computationally convenient to describe a system of clusters with a classical Hamiltonian

¹Even for structurally homogeneous systems the inner field will fluctuate at temperatures close to T_C .

§2.2. Density-functional theory

(Publication VII)

$$H_{\text{cl}} = - \sum_{i,j} J_{n_i n_j}(r_{ij}) \vec{S}'_i \cdot \vec{S}'_j - \sum_i E_{n_i}(S'_i), \quad (2.12)$$

where \vec{S}'_i denote the classical spins (S'_i varies between 0 and 1) of the i th cluster of n_i atoms, $J_{n_i n_j}(r_{ij})$ is an inter-cluster exchange parameter given as a function of inter-cluster separation r_{ij} , and $E_{n_i}(S'_i)$ denotes the internal energy of cluster i with spin S'_i . Total energies calculated for different spin configurations have to be mapped onto the Hamiltonian (2.12), and magnetic properties of macroscopic systems can be accessed via Monte Carlo simulations. In Publication VII we first calculate microscopic structures using Metropolis Monte Carlo method [70], followed by a two-stage simulation of the magnetic properties, where inter-cluster interactions are sampled using the Wolff algorithm [71] and the intra-cluster interactions using the Metropolis method.

§2.2 Density-functional theory

Calculating total energies of a many-electron system is cumbersome, as one needs to deal with both many-body effects as well as quantum effects. Exact solutions can only be obtained for system sizes up to just a few electrons, so for larger systems one has to be satisfied with numerical solutions. Hohenberg and Kohn have shown that the ground state energy of a system is uniquely given by the electron density [60]. The actual calculations follow the Kohn–Sham formalism [72] outlined below.

The full total energy functional of an interacting many-electron system reads [73, 74]

$$E[n_{\uparrow}(\vec{r}), n_{\downarrow}(\vec{r})] = \sum_{i\sigma}^{\text{occ}} \int d\vec{r} \Psi_{i\sigma}^* \left[-\frac{1}{2} \nabla^2 \right] \Psi_{i\sigma} + \int d\vec{r} n(\vec{r}) V_{\text{ion}} + \frac{1}{2} \int d\vec{r} \int d\vec{r}' \frac{n(\vec{r})n(\vec{r}')}{|\vec{r} - \vec{r}'|} + E_{\text{XC}}[n_{\uparrow}(\vec{r}), n_{\downarrow}(\vec{r})], \quad (2.13)$$

where $\Psi_{i\sigma}$ ($\sigma \in \{\uparrow, \downarrow\}$) are one-electron (Kohn–Sham) spin orbitals, V_{ion} is the ionic potential due to the nuclei, $n(\vec{r}) = n_{\uparrow}(\vec{r}) + n_{\downarrow}(\vec{r})$

2. Theoretical modeling

is the total electron density, and $E_{\text{XC}}[n_{\uparrow}(\vec{r}), n_{\downarrow}(\vec{r})]$ is the exchange-correlation (XC) energy as defined by Kohn and Sham [72]. (Here Hartree atomic units are used.) The total energy can be minimized using the Hohenberg–Kohn principle resulting in the Kohn–Sham constraint equation for the spin orbitals

$$\left[-\frac{1}{2}\nabla^2 + \underbrace{\left(V_{\text{ion}}(\vec{r}) + \int d\vec{r}' \frac{n(\vec{r}')}{|\vec{r} - \vec{r}'|} + V_{\text{XC}}^{\sigma}[n_{\uparrow}(\vec{r}), n_{\downarrow}(\vec{r})] \right)}_{V_{\text{eff}}^{\sigma}} \right] \Psi_{i\sigma} = \epsilon_{i\sigma} \Psi_{i\sigma}. \quad (2.14)$$

This constraint equation is of the form of an effective Schrödinger equation and gives Kohn–Sham spin orbitals in the effective potential V_{eff}^{σ} . This effective potential consists of the following three terms:

1. The first term V_{ion} represents the ionic potential caused by the positive ionic charges located at atomic positions.
2. The second term called the Hartree potential, represents the electron electrostatic potential and has the form

$$V_{\text{Hartree}} = \int_V d\vec{r}' \frac{n(\vec{r}')}{|\vec{r} - \vec{r}'|}, \quad (2.15)$$

where $n(\vec{r}) = n_{\uparrow}(\vec{r}) + n_{\downarrow}(\vec{r})$ is the total electron density

$$n(\vec{r}) = \sum_{\sigma} n_{\sigma}(\vec{r}) = \sum_{\sigma} \sum_{\text{states } i} f_{i\sigma} |\Psi_{i\sigma}(\vec{r})|^2. \quad (2.16)$$

$f_{i\sigma}$ is the occupation number of the spin orbital $\Psi_{i\sigma}(\vec{r})$.

3. The spin-dependent XC potential V_{XC}^{σ} is generally not known exactly. Formally V_{XC}^{σ} is defined as the functional derivative of the XC energy $E_{\text{XC}} = E_{\text{XC}}[n_{\uparrow}(\vec{r}), n_{\downarrow}(\vec{r})]$

$$V_{\text{XC}}^{\sigma}(\vec{r}) = \frac{\delta E_{\text{XC}}}{\delta n_{\sigma}(\vec{r})}. \quad (2.17)$$

The XC energy E_{XC} is defined in Eq. (2.13).

The many-electron problem has been mapped onto a set of single-electron Schrödinger like equations (2.14). By making some initial

§2.2. Density-functional theory

guess for the electron density n , the above Kohn–Sham equations (2.14) can be solved self-consistently. In principle we can obtain the exact ground state provided that V_{eff}^σ is known exactly. Unfortunately this is not the case and the XC term V_{XC}^σ must be approximated. The basic approximations used for the XC term and the wave function basis, implemented in the VASP code [62] are described below.

§2.2.1 XC functionals

The local density approximation (LDA) is a widely used scheme, which describes an XC energy at a point \vec{r} depending only on the electron density $n(\vec{r})$ at that point:

$$E_{\text{XC}}^{\text{LDA}} = \int d\vec{r} n(\vec{r}) \epsilon_{\text{XC}}(n(\vec{r})). \quad (2.18)$$

The XC energy per electron $\epsilon_{\text{XC}}(\vec{r})$ is approximated with the corresponding term describing a homogeneous electron gas. In the local spin density approximation (LSD) the XC potential is given by

$$V_{\text{XC}}^{\sigma, \text{LSD}}(\vec{r}) = \frac{\delta E_{\text{XC}}[n_\uparrow(\vec{r}), n_\downarrow(\vec{r})]}{\delta n_\sigma(\vec{r})}, \quad (2.19)$$

and the XC energy can be written as

$$E_{\text{XC}}^{\text{LSD}} = \int d\vec{r} n(\vec{r}) \epsilon_{\text{XC}}(n_\uparrow(\vec{r}), n_\downarrow(\vec{r})). \quad (2.20)$$

A more sophisticated approach is the generalized gradient approximation (GGA) in which also gradients of the electron density are included in the XC energy term. In GGA the XC energy is given by

$$E_{\text{XC}}^{\text{GGA}} = \int d\vec{r} f(n_\uparrow, n_\downarrow, \nabla n_\uparrow, \nabla n_\downarrow) \quad (2.21)$$

Here $f(n_\uparrow, n_\downarrow, \nabla n_\uparrow, \nabla n_\downarrow)$ is a function of the local spin densities and their gradients. There are several forms for $E_{\text{XC}}^{\text{GGA}}$. In this work the XC functional by Perdew and Wang (PW91 [75]) is used.

The above XC functionals based on the local density contain the so called self-interaction error [74]. An improvement to the above local approximations can be made by the on-site Coulomb correction U [76, 77], which however is a parameter which cannot be determined unambiguously. To study the effects of these corrections, in Publication VI we also use the LSD+ U functional.

§2.2.2 The projector augmented–wave method

Solving numerically the Kohn–Sham equations (2.14), it is convenient to describe the orbital part of $\Psi_{i\sigma}$ (henceforth simply called wave function $|\Psi\rangle$) as an expansion onto some set of basis functions. The behavior of the wave function in different regions of space varies considerably, and finding a universal set of basis functions is cumbersome. In Publication I various computational methods are compared, and the projector augmented–wave method is found to be the most suitable one for the modeling of magnetic semiconductors. In augmented–wave methods, space is divided into regions based on physical arguments: around atomic nuclei (known as the augmentation region Ω_R) the wave function oscillates rapidly, and it is convenient to expand the wave function as partial waves (spherical harmonics); while in the region between atoms outside the nuclei (called interstitial region), i.e. outside Ω_R , the wave function behaves rather smoothly so that envelope functions expanded into e.g. plane waves are convenient. Following the notation used by Bloechl [61], the wave function reads

$$|\Psi\rangle = \begin{cases} |\psi^{\text{PW}}\rangle = \sum_G c_G |e^{i\vec{G}\cdot\vec{r}}\rangle & \text{outside } \Omega_R \\ \sum_i a_i |\phi_i\rangle & \text{inside } \Omega_R, \end{cases} \quad (2.22)$$

where $|\psi^{\text{PW}}\rangle$ is the plane wave expansion and $|\phi_i\rangle$ are atomic partial waves.² Naturally the wave function must be continuous and differentiable at the augmentation–interstitial border, and further, the plane wave part of the wave function should vanish inside the augmentation spheres.

In the projector–augmented wave method introduced by Bloechl [61] the wave functions are linearly transformed into auxiliary functions (denoted with the tilde ‘ $\tilde{\sim}$ ’) $|\Psi\rangle = T|\tilde{\Psi}\rangle$ with rapidly converging plane wave coefficients, so the entire system can be described using solely a plane wave basis. Because the interstitial region already behaves smoothly, the transformation should be of the form

$$T = 1 + \sum_R T_R, \quad (2.23)$$

²Here $|\phi_i\rangle$ is a short-hand notation for $|\phi_{\vec{R},l,m,n}\rangle$, where \vec{R} denotes atomic site, $L = (l, m)$ the angular momentum quantum numbers and n is an additional index to label different partial waves on the same site.

§2.2. Density-functional theory

where T_R is a local operator. For each partial wave $|\phi_i\rangle$ a corresponding auxiliary function $|\tilde{\phi}_i\rangle$ is chosen such that

$$\begin{aligned} T_R|\tilde{\phi}_i\rangle &= |\phi_i\rangle - |\tilde{\phi}_i\rangle, \\ |\psi^{\text{PW}}\rangle &= \sum_i a_i |\tilde{\phi}_i\rangle \quad \text{inside } \Omega_R, \text{ and} \\ |\tilde{\phi}_i\rangle &= |\phi_i\rangle \quad \text{outside } \Omega_R. \end{aligned} \quad (2.24)$$

Now the total wave function can be written as

$$|\Psi\rangle = |\psi^{\text{PW}}\rangle + \sum_i a_i \left(|\phi_i\rangle - |\tilde{\phi}_i\rangle \right). \quad (2.25)$$

We introduce a set of projector functions $|\tilde{p}_i\rangle$, to expand the auxiliary wave function $|\tilde{\Psi}\rangle$ in terms of the auxiliary partial waves $|\tilde{\phi}_i\rangle$, so we may write

$$|\tilde{\Psi}\rangle = \sum_i \langle \tilde{p}_i | \tilde{\Psi} \rangle |\tilde{\phi}_i\rangle \quad \text{inside } \Omega_R. \quad (2.26)$$

These projector functions need to fulfill the completeness relation $\sum_i |\tilde{\phi}_i\rangle \langle \tilde{p}_i| = 1$, which further implies orthonormality $\langle \tilde{p}_i | \tilde{\phi}_j \rangle = \delta_{i,j}$. Using this completeness relation, the plane wave part inside augmentation region can be written as

$$|\psi^{\text{PW}}\rangle = \sum_i |\tilde{\phi}_i\rangle \langle \tilde{p}_i | \psi^{\text{PW}} \rangle = \sum_i \langle \tilde{p}_i | \psi^{\text{PW}} \rangle |\tilde{\phi}_i\rangle \quad \text{inside } \Omega_R. \quad (2.27)$$

Comparing this with the previous expression for the plane wave part (Eq. 2.24) the coefficients a_i are identified as overlap integrals of the projector functions $\langle \tilde{p}_i|$ and the interstitial region wave function $|\psi^{\text{PW}}\rangle$:

$$a_i = \langle \tilde{p}_i | \psi^{\text{PW}} \rangle. \quad (2.28)$$

Finally, the total wave function (2.25) gets the form

$$|\Psi\rangle = |\psi^{\text{PW}}\rangle + \sum_i \langle \tilde{p}_i | \psi^{\text{PW}} \rangle \left(|\phi_i\rangle - |\tilde{\phi}_i\rangle \right). \quad (2.29)$$

Here the total wave function is expressed only in terms of the projector functions, the plane wave basis, and the physical and auxiliary partial waves.

§2.2.3 Total energy calculations

The density-functional calculations presented in this thesis are carried out using the Vienna *ab initio* simulation package VASP [62]. The Kohn–Sham equations (2.14) are solved self-consistently beginning from some initial spin densities n_σ^0 . These initial spin densities also define the effective potential V_{eff}^σ , and the spin orbitals $\Psi_{i\sigma}$ are solved from the Kohn–Sham equations. New spin densities $n_\sigma^{1'}$ and the corresponding total energy can be calculated from equations (2.16) and (2.13), respectively. $n_\sigma^{1'}$ could be used directly as the initial spin densities for the next iteration cycle, but instead usually the new spin densities n_σ^1 are generated by mixing $n_\sigma^{1'}$ and n_σ^0 (we use the Broyden and Kerker mixing schemes [62]), and equations (2.16) and (2.13) are solved as above. This iteration is continued until a self-consistent solution is found, i.e. the total energy during cycle $j + 1$ changes less than some predefined tolerance energy E_{break} : $E^j - E^{j+1} < E_{\text{break}}$ (here $E_{\text{break}} = 10^{-4}$ eV).

Total energies can be easily calculated for a number of configurations. For example binding energies E_b are calculated by comparing the total energies of different geometrical configurations. Besides different geometrical configurations, also magnetic ones can be calculated by giving the appropriate initial spin densities. Typically we calculate both ferromagnetic spin configurations ‘F’ and antiparallel spin alignments ‘A’—the total energy difference $E^{\text{A}} - E^{\text{F}}$ then yields the spin-flip energy Δ .

CHAPTER 3

(Ga,Mn)As

This chapter overviews Publications I–V for (Ga,Mn)As. First, results considering the microscopic structure and cluster formation are presented, followed by a discussion on magnetic coupling. The atomic scale interactions and band structures are calculated from first principles using the VASP code [62] in supercells of 64–128 atoms. The experimental lattice constant of $a = 5.65 \text{ \AA}$ is used throughout together with a plane wave basis up to the cut-off energy of 275 eV and a Monkhorst–Pack \vec{k} -mesh with \vec{k} -point density of $(0.14 \text{ \AA}^{-1})^3$. Large scale cluster distributions are calculated using kinetic Monte Carlo methods. The Curie temperature is approximated with the Weiss molecular field theory.

§3.1 Microscopic structure

The energetically most favorable configurations consist of nearest neighbor substitutional Mn_{Ga} 's in ferromagnetic high symmetry configurations, as shown in Publications I–IV. The first principles calculations describe the experimentally relevant Mn concentrations of $[\text{Mn}] = 6.3 \%$, with the exception of five substitutional Mn atoms in the supercell corresponding to $[\text{Mn}] = 7.8 \%$. The energetically most important Mn cluster configurations are shown in Fig. 3.1. For the cases of 2–4 Mn atoms in the supercell the configuration where the Mn atoms share the *same neighbouring* As site is always found to be energetically most favorable (see the upper left-hand corners in Figs 3.1 (a)–(c)). Also, it is energetically favorable to form one cluster from two separate components in all cases shown in Figs 3.1 (a)–(c).

3. $(Ga, Mn)As$

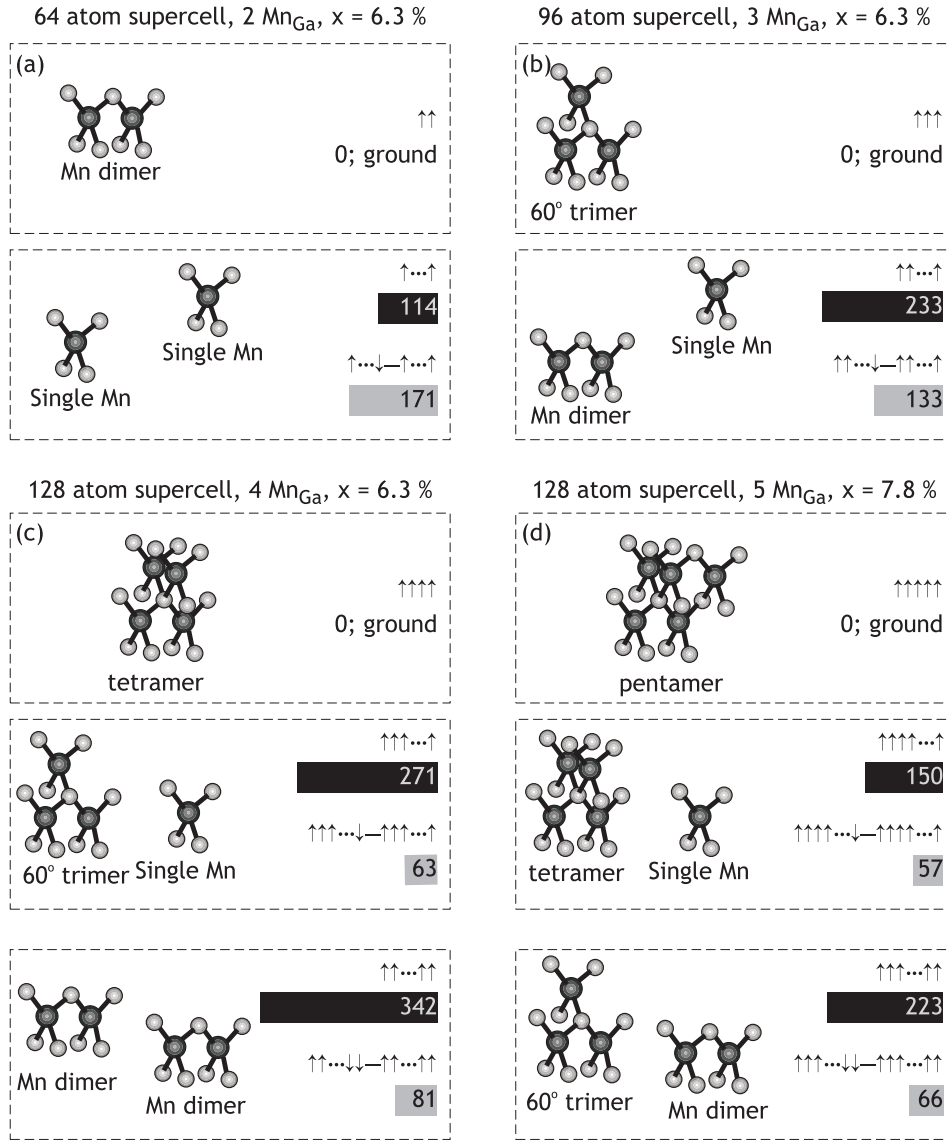


Figure 3.1. [From Publication IV] Calculated Mn cluster configurations and total energies. The dark and gray balls denote the Mn and As atoms, respectively. Separated components are placed at the maximum distance available. All the black horizontal bars show the (ferromagnetic) separation (or binding) energies; the corresponding values are given in the units of meV in the black bars. The gray horizontal bars with the arrow diagrams show the spin-flip energies; the corresponding values are given in the units of meV inside the gray bars. All the black and gray horizontal bars are drawn in the same scale.

§3.1. Microscopic structure

In the case of five Mn atoms in the supercell the energetically most favorable configuration is obtained by attaching the fifth Mn atom to the stable tetramer [Fig. 3.1 (d)]. The energies needed to separate single clusters into two components (or the binding energies for the components) are shown graphically in Fig. 3.1 as black horizontal bars which contain also the corresponding energy values in the units of meV. In all these cases the ferromagnetic order is the stablest magnetic phase.

The binding of a Mn_{Ga} atom to a cluster can to good accuracy be estimated from the dimer binding energy $E_b (= 0.1 \text{ eV})$ [see Fig. 3.1 (a)] as $n \cdot E_b$, where n is the number of nearest neighbor Mn_{Ga} atoms in the resulting cluster. Consequently, the lowest energy microstructure is composed of Mn clusters instead of separated single Mn_{Ga} , or even of second phase precipitates for very high Mn concentrations. However, to approach this lowest energy microstructure within reasonable time requires an efficient diffusion mechanism for the substitutional Mn_{Ga} atoms, which is discussed below.

§3.1.1 Kinetic considerations

As shown in Publication V, Mn_{Ga} may diffuse on the Ga sublattice using Ga vacancies as a vessel of migration. This diffusion leads to the Mn clustering discussed above. Although the formation of Mn_{Ga} clusters is energetically favorable as shown above and in Ref. [28], it requires an abundance of mobile vacancies. The gallium vacancy (V_{Ga}) concentrations in (Ga,Mn)As up to 10^{18} cm^{-3} [78] are rather high, and our combined density-functional theory and kinetic Monte Carlo study yields that these vacancies actually are mobile at the relevant temperatures.

The vacancy mediated substitutional Mn migration over the Ga-sublattice illustrated in Fig. 3.2 consists of the following three steps: (i) the Mn_{Ga} atom and a vacancy form a pair; (ii) the Mn_{Ga} atom and the vacancy exchange places; and (iii) the pair dissociates. To understand this pair formation-dissociation mechanism we calculate from first principles the migration energy for V_{Ga} , the migration barrier for the $\text{Mn} \rightarrow V_{\text{Ga}}$ transition, and the $\text{Mn}-V_{\text{Ga}}$ interaction potential (i.e. binding energy).

In contrast to the $\text{Mn}_{\text{Ga}}-\text{Mn}_{\text{Ga}}$ interaction, bringing together a Mn_{Ga}

3. (Ga,Mn)As

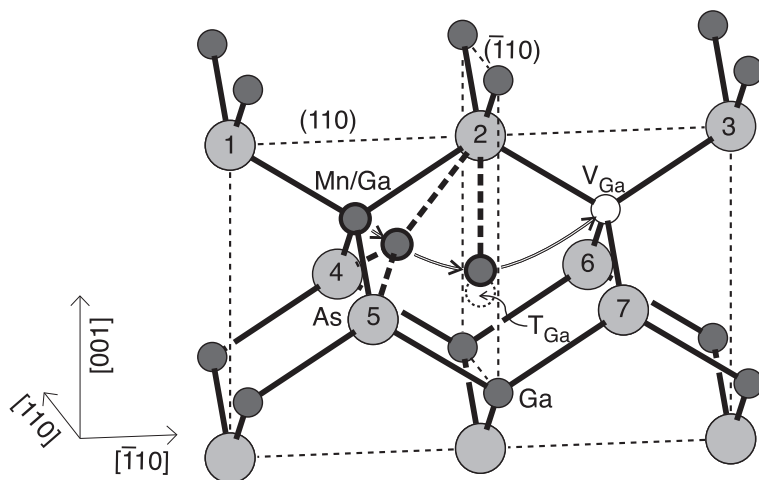


Figure 3.2. [From Publication V] Schematic representation of the Mn/Ga migration path. The intermediate stages, where the Mn/Ga atom is in a planar configuration with surrounding As atoms 2, 4, and 5, and where the Mn/Ga atom passes through the $(\bar{1}10)$ plane close to the T_{Ga} interstitial site are also given, and bonds in these configurations are denoted with the thick dashed lines.

and a V_{Ga} is energetically unfavorable and costs 0.2 eV, i.e. $E_b = -0.2$ eV. The negative binding energy means that the pair dissociation barrier will be 0.2 eV lower than the pair formation barrier. Nonetheless, such pairs may be formed kinetically if the formation barrier is reasonably low. The efficiency of the vacancy mediated diffusion is determined by the relation of the activation barriers for direct $\text{Mn}_{\text{Ga}} \leftrightarrow V_{\text{Ga}}$ exchange and $\text{Mn}_{\text{Ga}}-V_{\text{Ga}}$ pair formation-dissociation processes.

The migration barriers obtained in Publication V are 1.6 eV and 0.8 eV for the Ga and Mn migration, respectively.¹ Although the Mn rich metallic environment studied in this work differs from pure GaAs, the migration barrier for the vacancy mediated Ga self-diffusion of 1.6 eV is well in agreement with the first principles calculation for a neutral vacancy [79], and also with the experimental values around 1.5-1.9 eV [80–82] in pure GaAs (Table 3.1). Considering the barriers given above, the probability of the $\text{Mn}_{\text{Ga}}-V_{\text{Ga}}$ exchange vs. the V_{Ga} migration jump differs at relevant growth and annealing temperatures of around 250°C by a factor of 10^7 . For the dissociation of a $\text{Mn}_{\text{Ga}}-V_{\text{Ga}}$ we obtain an activation barrier of 1.4 eV by combining the V_{Ga}

¹These barriers may be overestimated, because only nearest neighbor atoms are allowed to relax as described in more detail in Publication V.

§3.1. Microscopic structure

Table 3.1. [From Publication V] Migration barriers Q_b for Ga-self diffusion and Mn diffusion via the Ga monovacancy mechanism. PWPP denotes the plane wave pseudopotential method, and Expt experiment.

Process	Q_b (eV)	PWPP (eV)	Expt (eV)
Ga \rightarrow V_{Ga}	1.6	1.7 ^a	1.5-1.9 ^b
Mn _{Ga} \rightarrow V_{Ga}	0.8		

^a [79], ^b [80–82].

migration barrier with the negative Mn_{Ga}– V_{Ga} binding energy. The Boltzmann factor for this dissociation barrier is 100 times larger than that for the V_{Ga} migration barrier, but still 10^5 times smaller than the Mn_{Ga}– V_{Ga} exchange probability. Therefore the bottleneck for Mn_{Ga} diffusion via the pair formation–dissociation mechanism is the mobility of V_{Ga} . However, at large Mn_{Ga} concentrations, Mn_{Ga}– V_{Ga} pairs are formed more frequently, and due to the low pair dissociation and exchange barriers the V_{Ga} diffusivity is expected to increase.

The pairwise binding energies ² and migration energies (Table 3.1) are used to study structural evolution with lattice kinetic Monte Carlo simulations using the Casino-LKMC code [83]. The number of clusters as a function of annealing time and temperature are given in Fig. 3.3. The Mn–Mn attraction combined with efficient Mn diffusion at increasing temperatures of 250°C or higher leads to increasing clustering. The clustering rate exhibits typical Arrhenius dependence, i.e. the logarithm of the clustering rate depends linearly on the inverse temperature. Further, an increase in Mn concentration increases the clustering rate as well, because fewer migration jumps are required for Mn to reach another Mn atom. At the same time significant clustering starts to occur at lower temperatures. This behavior is seen explicitly in Figs 3.3 (a) and (b), and the sensitive temperature dependence is seen for [Mn] = 5 % in Figs 3.3 (c) and (d). A similar rapid clustering occurs as the Mn concentration increases from 5 % to 8 % even at 250°C. Thus at these large concentrations significant clustering will occur already during growth, which takes a few hours [2]. Furthermore, the increasing number of large clusters may lead to formation

²The cluster binding energies are slightly overestimated in the approximation based solely on pair interactions—cf. Publications II and III. Therefore using the pairwise interaction approximation may overstate the number of large clusters.

3. $(Ga,Mn)As$

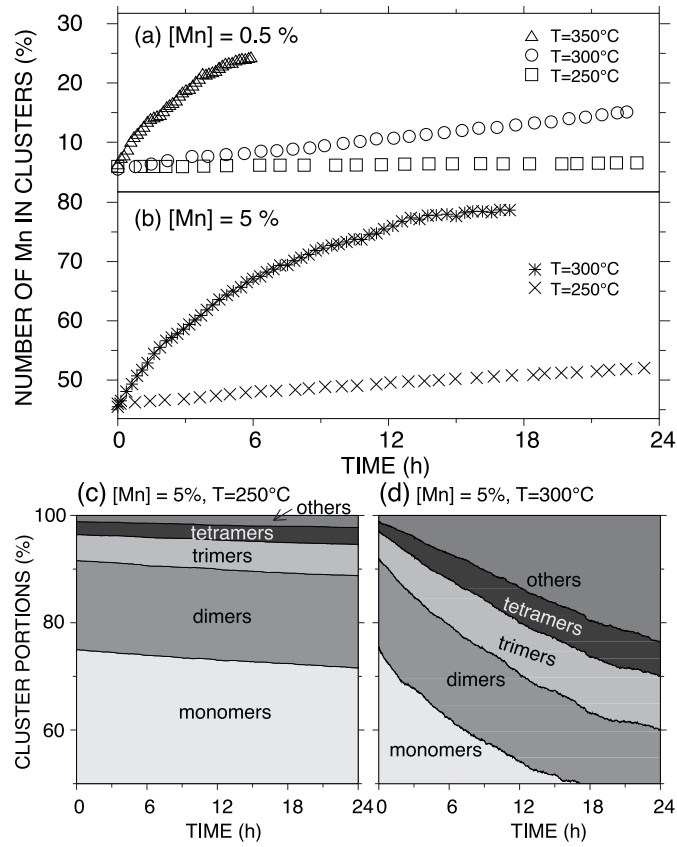


Figure 3.3. [From Publication V] Percentage of Mn atoms included in clusters as a function of annealing time for the Mn concentrations of 0.5 % (a) and 5 % (b), and cluster portion percentages for the Mn concentration of 5 % as a function of annealing time corresponding to temperatures of 250°C (c) and 300°C (d).

of a secondary MnAs phase with the NiAs structure, as observed in growth of $(Ga,Mn)As$ samples with Mn concentrations beyond 7 % [2].

§3.2 Band structure

The density of states (DOS) together with the branching diagram for a uniform substitutional Mn distribution in our dilute limit of $x = 1.6\%$ (or one substitutional Mn atom in the 128 atom supercell) is shown in Fig. 3.4. The most important feature of the DOS is the single hump in the majority spin (\uparrow) channel at the Fermi level (E_F) which makes (Mn,Ga)As a half-metal (Figs 3.4 (b) and (c)). The hump is formed mainly from the $t_{a\uparrow}$ antibonding states (Fig. 3.4 (a)). Each Mn atom contributes one hole state in the unoccupied part of the hump as well as the net magnetic moment of $4\mu_B$ [two e_{\uparrow} and two $t_{a\uparrow}$ electrons, see Fig. 3.4 (a)] (μ_B is the Bohr magneton).

The dilute-limit majority-spin hump at the Fermi energy E_F in Fig. 3.4 (c) is found to split when Mn clusters are formed, and new narrower unoccupied bands appear in the gap. This is shown for the Mn monomer, dimer, trimer, and tetramer systems at the constant Mn concentration of $x = 6.3\%$ in Fig. 3.5. At the same time the hole density grows at the As atom which is situated in the center of the Mn cluster. This was shown for the Mn dimer in Publications I and IV and a similar splitting is also found in Ref. [29]. The increasing localization at the center As atom is reflected in the increasing separation and size of the split-off part of the hump in Fig. 3.5. The As

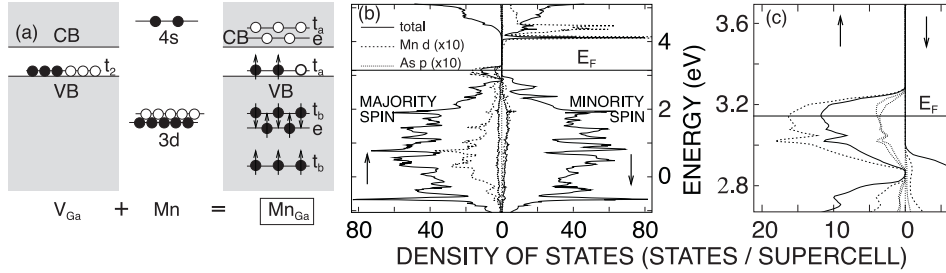


Figure 3.4. [From Publication IV] The calculated density of states (DOS) for the Mn concentration of $x = 1.6\%$. (a) Branching diagram for a substitutional Mn atom. The states of the substitutional Mn atom are formed via the hybridization of the $V_{Ga} t_2$ and Mn $3d$ states. (b) DOS. E_F denotes the Fermi level. The dashed and dotted lines give the site and orbital projected DOS. (c) The magnification of the DOS around E_F .

3. $(Ga,Mn)As$

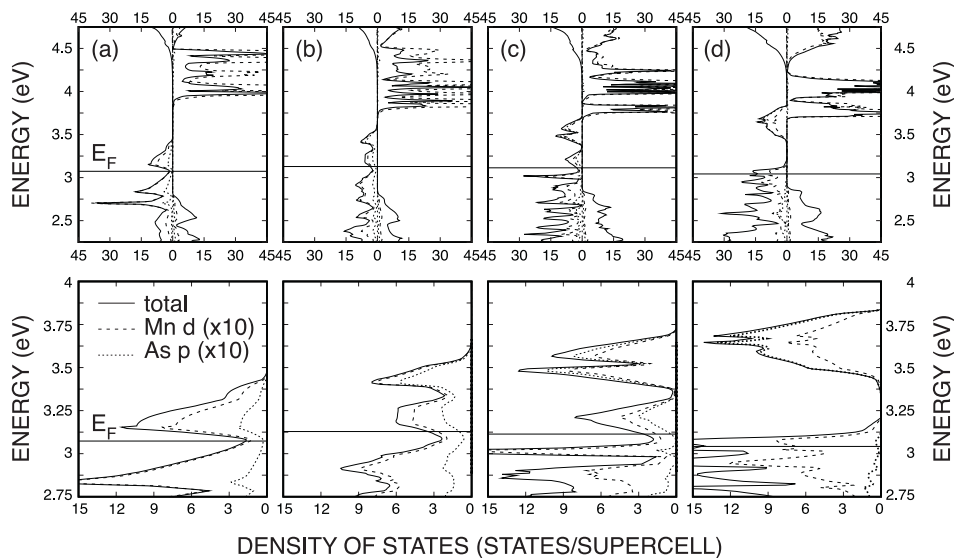


Figure 3.5. [From Publication IV] Densities of states (DOSs) around the band gap (upper figures) and the magnifications of the majority spin DOSs around the Fermi energy (E_F) (lower figures). The dashed and dotted lines give the site and orbital projected DOS. Figures (a), (b), (c), and (d) give the DOSs for the Mn monomer, dimer, trimer, and tetramer, respectively for the Mn density of $x = 6.3\%$.

p -projection in the split-off part of the hole DOS is seen to increase in relation to the Mn d -projection in Fig. 3.5 and even to exceed the Mn d projection in the cases of the Mn trimer and tetramer [Figs 3.5 (c) and (d)].

Along the band splitting the unoccupied As p states (hole states) become increasingly localized inside the Mn cluster. The total number of holes induced by a cluster of N Mn atoms is N , but approximately $N - 1$ holes get localized *inside the cluster*. Therefore, effectively one cluster contributes only one mobile hole *outside the cluster* regardless of the cluster size. The As p component of the spin-polarized hole density as a function of the distance to the closest Mn atom is shown in Fig. 3.6 for several different cluster sizes. At short distances $r < 7 \text{ \AA}$ to the closest Mn atom of the cluster, the hole concentration increases with increasing number of Mn atoms. However, for larger distances $r > 7 \text{ \AA}$ the hole concentrations approach approximately the same curve. Therefore, the long-distance magnetic coupling between the

§3.3. Curie temperature

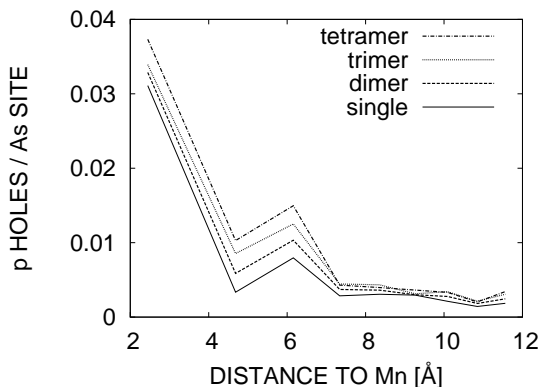


Figure 3.6. [From Publication IV] The As p hole distribution for different cluster sizes. The average number of p holes per As site at each As coordination cell is given. The numbers are obtained by integration from the orbital decomposition. Although the orbital decomposition as well as the choice of the integration volume are not unambiguous, the relative magnitudes are directly comparable.

Mn clusters depends only on their mutual distance, not on the size of the cluster, and thus the cluster–cluster exchange interaction is well described with a single exchange coefficient J_{ij} (cf. Eq. 2.10).

§3.3 Curie temperature

As mentioned in §3.1, the ferromagnetic alignment is always energetically most stable compared with other magnetic alignments. Because of the strong increase in the p – d hybridization inside a Mn cluster both the bonding and the magnetic interaction inside the clusters are strong. This is also reflected in the strong intra-cluster spin-flip energies typically of around 200 meV or more, which yield large critical temperatures of around 500–1000 K for the magnetic ordering inside the clusters (see Publication III). This indicates that the Curie temperature of (Ga,Mn)As will be given by the cluster–cluster (inter-cluster) exchange interactions, which are characterized by the smaller spin-flip energies Δ given in Fig. 3.1.

The Curie temperatures calculated using Eq. (2.9)

$$T_C = \frac{2\Delta'}{3k_B}$$

corresponding to various cluster–cluster systems, are given in Table 3.2. Notice that the energy values Δ in Fig. 3.1 correspond to energy difference per supercell, and as one supercell contains two clusters, one

3. (Ga,Mn)As

Table 3.2. [From Publications III and IV] Curie temperatures from inter-cluster spin-flip energies for supercells containing two Mn clusters calculated from the energy difference between anti-parallel (A) and ferromagnetic (FM) spin states. [Mn] and [cl] denote the Mn and cluster concentrations, respectively.

System	FM	A	T_C (K)	[Mn] (%)	[cl] (%)
Mn ₁ +Mn ₁	↑ · ↑	↑ · ↓	660	6.3	6.3
Mn ₂ +Mn ₁	↑↑ · ↑	↑↑ · ↓	514	6.3	4.1
Mn ₁ +Mn ₁	↑ · ↑	↑ · ↓	220	3.1	3.1
Mn ₂ +Mn ₁	↑↑ · ↑	↑↑ · ↓	282	4.7	3.1
Mn ₃ +Mn ₁	↑↑↑ · ↑	↑↑↑ · ↓	244	6.3	3.1
Mn ₂ +Mn ₂	↑↑ · ↑↑	↑↑ · ↓↓	313	6.3	3.1
Mn ₄ +Mn ₁	↑↑↑↑ · ↑	↑↑↑↑ · ↓	220	7.8	3.1
Mn ₃ +Mn ₂	↑↑↑ · ↑↑	↑↑↑ · ↓↓	255	7.8	3.1

should use $\Delta' = \Delta/2$ in estimating the Curie temperatures. One immediately notices for the fixed cluster concentration of [cl] = 3.1 % that although the Mn concentration varies between 3.1–7.8 %, the Curie temperature remains more or less constant. Furthermore, T_C grows as the cluster concentration increases. This behavior shows that in (Ga,Mn)As the Curie temperature is determined by the cluster concentration instead of the Mn concentration.

The Curie temperature in the Weiss molecular field theory is proportional to the energy Δ that corresponds to the spin-flip energy of one Mn cluster. On the other hand, we recall from Eq. (2.8) that Δ is proportional to the sum of exchange interactions $\sum_i J_{i0}$, which may be assumed to decay rapidly. As Mn clusters are formed, the total number of clusters or cluster concentration naturally decreases, and so will also decrease the sum $\sum_i J_{i0}$. Therefore increasing clustering will inevitably reduce T_C . Recalling Eq. (2.1), the Curie temperature according to the Weiss model actually is directly proportional to the number of magnetic particles N , i.e. $T_C \propto [\text{cl}]$.

The actual cluster concentration in experimental samples has not been measured to date, but cluster distributions and cluster concentrations can be calculated e.g. using kinetic Monte Carlo methods, as discussed in §3.1. The calculated cluster distributions given in Fig. 3.3 at the Mn concentration of [Mn] = 5 % correspond to cluster configurations

§3.3. Curie temperature

ranging from 3.6 (as-grown) to 3.3 % (annealed for 24 h at 250°C). Using a linear expression for T_C based on the data in Table 3.2 the cluster concentrations $[cl] = 3.3\text{--}3.6\%$ would correspond to a T_C of 270–320 ± 50 K. Present high-quality (Ga,Mn)As samples where the amount of the harmful interstitial Mn and As_{Ga} defects has been minimized yield T_C 's in the range of 159–173 K [33, 34]. The theoretically estimated Curie temperatures are expectedly overestimated, because the model excludes the compensation effect due to As_{Ga} antisites and neglects magnetic fluctuations. Nonetheless, the T_C values of around 300° may be regarded as an upper limit for an ideal uncompensated sample with $[Mn] \approx 5\%$, and the T_C decrease of about 40 K due to thermal annealing at 250°C for 24 h agrees closely with experiment [40, 42].

CHAPTER 4

(Ga,Mn)N

This chapter overviews Publications VI and VII for (Ga,Mn)N. The microstructure is obtained from first principles binding energies of substitutional Mn atoms combined with Metropolis Monte Carlo (MC) simulations. In the VASP calculations carried out in 48–108 atom supercells representing the wurtzite structure with lattice optimized parameters $a = 3.217 \text{ \AA}$ and $c : a = 1.631$. The plane wave cutoff energy is 425 eV, and the \vec{k} -point sampling is modified according to supercell size keeping the sampling density roughly uniform, as described in Publication VI. Both the mean field theory and Monte Carlo methods are used to estimate Curie temperatures for (Ga,Mn)N.

§4.1 Microscopic structure

Two different Mn cluster distributions are considered: a fully random distribution and a distribution in thermal equilibrium at 1000 K. The former is obtained simply by randomly substituting Ga atoms by Mn atoms, and the latter is obtained from a Metropolis MC simulation [70] using the *ab initio* binding energies given in Table 4.1. Notice that the Mn binding energy values are significantly larger than those in

	ΔE (meV)
$\text{Mn}_1 + \text{Mn}_1 \longleftrightarrow \text{Mn}_2$	521
$\text{Mn}_1 + \text{Mn}_2 \longleftrightarrow \text{Mn}_3$	615
$\text{Mn}_1 + \text{Mn}_3 \longleftrightarrow \text{Mn}_4$	622

Table 4.1. [From Publication VII] Monomer-cluster binding energies. These binding energies are calculated using 72 atom supercells as described in Publication VI.

4. $(\text{Ga}, \text{Mn})\text{N}$

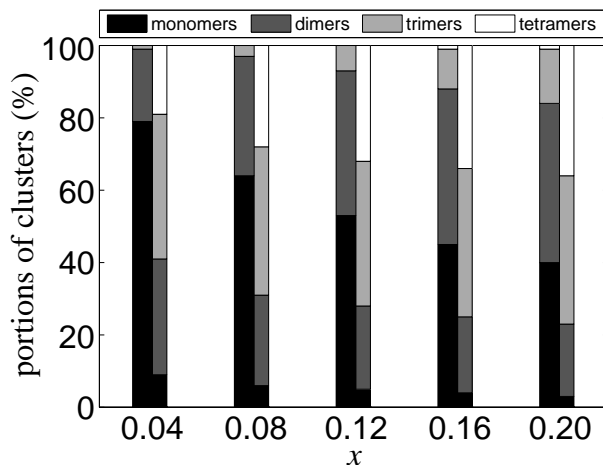


Figure 4.1. [From Publication VII] Percentage portions of clusters in the case of random distribution of substitutional Mn atoms (wide left columns) and in the case of thermal equilibrium at $T = 1000$ K (narrow right columns).

$(\text{Ga}, \text{Mn})\text{As}$, so one may expect the clustering effect in $(\text{Ga}, \text{Mn})\text{N}$ to be stronger. Nonetheless, one should keep in mind that the realistic Mn distribution lies somewhere between the fully random and thermal equilibrium, and computationally it can only be found by taking kinetic considerations into account (cf §3.1.1).

The cluster portions for the random and equilibrium distributions are given in Fig. 4.1 as a function of Mn concentration $[\text{Mn}]$. In the case of the random distribution (left wide columns) one immediately notices the relatively large dimer portion at large $[\text{Mn}]$ while the trimer portion and especially the tetramer portion remain small. In the case of the thermal equilibrium distribution at 1000 K (right narrow columns) considerable clustering has taken place: almost all monomers have vanished and the portion of dimers has considerably diminished, while the portion of the trimers and especially that of the tetramers have grown markedly. Therefore also in order to understand the magnetic properties of $(\text{Ga}, \text{Mn})\text{N}$ clustering effects cannot be neglected—clustering effects on the band structure as well as on the magnetic coupling need to be investigated.

§4.2. Band structure and magnetic properties

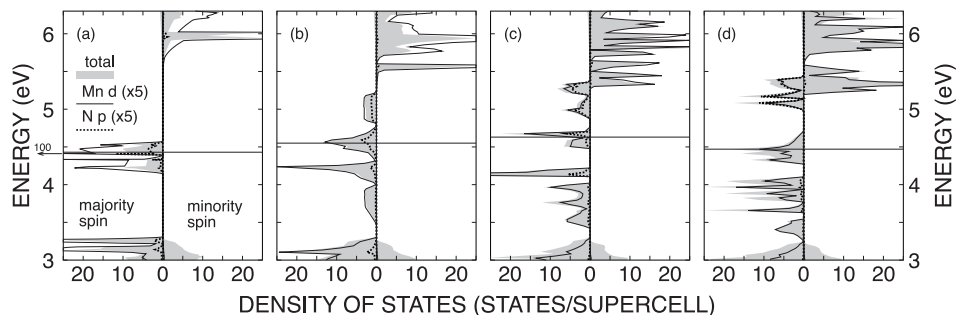


Figure 4.2. [Partially from Publication VI] GaN density of states (DOS): Clustering induced splitting of the DOS at the Fermi level E_F . The panels from left to right represent a Mn monomer, dimer, trimer and tetramer, corresponding to Mn concentrations of 2.8 %, 5.6%, 8.3 % and 11.1 %, respectively.

§4.2 Band structure and magnetic properties

The band splitting developments in (Ga,Mn)N given in Fig. 4.2 are similar to those in (Ga,Mn)As (cf. Fig. 3.5 and discussion in §3.2), but as the impurity states initially are different, so are the effects and consequences of band splitting, too. In (Ga,Mn)N the Mn induced acceptor level is mid-gap, and thus corresponds to a strongly *localized* Mn *d* hole. The clustering induces shallow, more *delocalized* hole states that will strengthen hole mediated ferromagnetism. On the other hand, simultaneously the acceptor levels with the anti-parallel spin-alignment also become split, which strengthens anti-ferromagnetic interactions eventually cancelling the ferromagnetic interactions. The effects on magnetism are described in more detail below.

§4.2.1 Molecular field theory

First the Curie temperatures are determined directly from the first principles calculations for different cluster configurations using Eq. (2.9). The calculated spin-flip energies together with estimated T_C values are given in Table 4.2. The T_C of monomer–monomer systems exhibits very strong dependence on Mn concentration [Mn]. Dimer formation

4. $(Ga,Mn)N$

Table 4.2. [From Publication VI] Spin-flip energies (Δ) and mean field approximation Curie temperatures (T_C) for two clusters in the supercell. The fourth and fifth columns are GGA calculations, the sixth and seventh columns LSD+ U calculations (denoted by the index “+ U ”). d is the minimum distance between the Mn atoms belonging to the different centers.

System	x (%)	d (Å)	Δ (meV)	T_C (K)	Δ^{+U}	T_C^{+U}
Mn ₁ - Mn ₁ ^a	5.6	7.65	10	39	1	4
Mn ₁ - Mn ₁ ^b	8.3	6.15	92	355	-	-
Mn ₂ - Mn ₁ ^a	8.3	6.13	133	514	160	618
Mn ₃ - Mn ₁ ^a	11.1	6.13	76	294	117	453
Mn ₃ - Mn ₁ ^c	7.4	9.28	33	128	-	-
Mn ₄ - Mn ₁ ^c	9.3	7.66	7	27	10	39
Mn ₄ - Mn ₃ ^c	13.0	6.19	1	4	-	-

^a 72 atoms/supercell (SC), ^b 48 atoms/ SC, ^c 108 atoms/SC

appears to increase T_C significantly, but trimer and tetramer formation again reduces T_C compared with dimer systems, the tetramer configurations exhibiting a T_C of virtually zero.

The increase in the Curie temperature for the dimer configurations is due to the increased delocalization of the impurity band shown in Fig. 4.2. The lowering of T_C for the larger clusters on the other hand is due to the increased splitting of the impurity levels that in turn changes the $p-d$ hybridization around Fermi level seen pronouncedly in Fig. 4.2 (d). The mean field estimate T_C depends very sensitively on cluster size and geometry, and as actual systems consist of a mixture of different size clusters, some kind of averaging of different cluster configurations could give more realistic T_C estimates. A straightforward approach—presented in Publication VII—based on Monte Carlo methods is described below.

§4.2.2 Monte Carlo simulations

The magnetic interactions are modeled using the classical Hamiltonian

$$H = - \sum_{i,j} J_{n_i n_j}(r_{ij}) \vec{S}_i \cdot \vec{S}_j - \sum_i E_{n_i}(S_i), \quad (\text{Eq. 2.12})$$

where the functions $E_{n_i}(S_i)$ are constructed from intra-cluster energies, and the $J_{n_i n_j}(r_{ij})$ are obtained by fitting H to first principles inter-cluster spin flip energies as described in Publication VII. First the J_{12} are fitted for the monomer-dimer pair for which a high spin-flip energy was obtained (see Table 4.2). The fit is done on ten *ab initio* values calculated at different separations. From various functional forms r^{-3} most naturally describes the general behaviour. The best fit is then obtained by choosing a function composed of the decaying r^{-3} -term and a local term describing a peak at 6 Å:

$$\frac{A}{r^3} + B(r - r_1)e^{-\alpha(r-r_2)^2}, \quad (4.1)$$

where A , B , r_1 , α , and r_2 are constants. This same form is then chosen for the other cluster pairs as well, and the local term is assumed to be of the same shape i.e. α , $r_2 - r_1$, and Br_1^3/A are kept the same for all cluster pairs. The remaining coefficients A and r_1 are fitted independently for all other cluster pairs using 2-3 calculated *ab initio* values. In the supercell density-functional calculation the cluster-cluster separation reaches up to 11 Å, but in the fitting also the coupling to periodic images is included up to the cut-off radius of 13 Å ($\approx 4a$). This cut-off is also used throughout the MC simulations, i.e. the magnetic coupling beyond 13 Å equals zero. Figure 4.3 shows the resulting ten $J_{n_i n_j}$ exchange coefficients needed to describe the magnetic interactions. Notice that

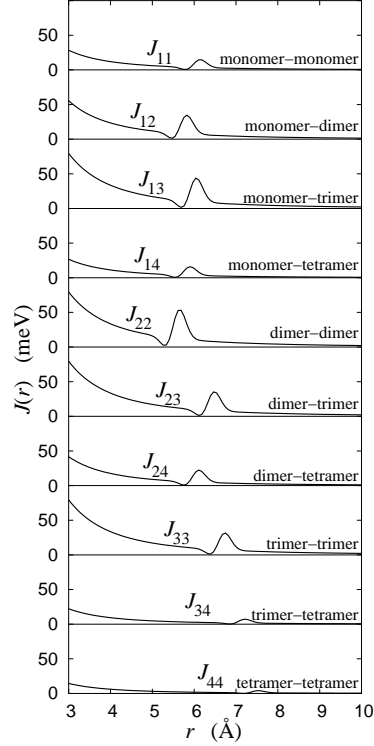


Figure 4.3. [From Publication VII] Intercluster exchange constants $J_{n_i n_j}$. The distance is measured between the centers of mass of the Mn atoms of the two clusters.

4. $(Ga,Mn)N$

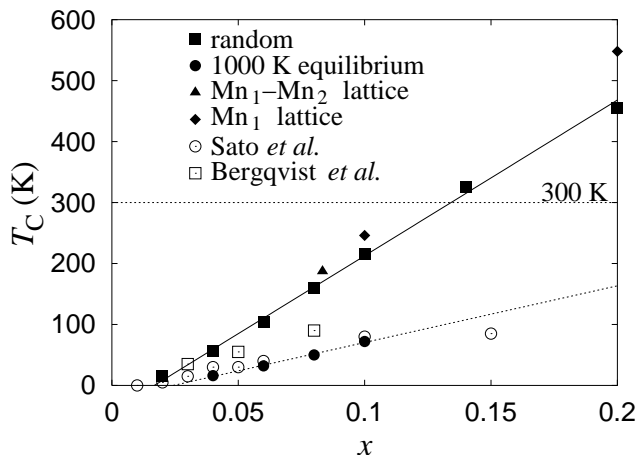


Figure 4.4. [From Publication VII] Curie temperatures T_C for the random substitutional Mn distribution (filled squares), the thermal equilibrium Mn distribution at 1000 K (filled circles), the regular monomer-dimer lattice (filled triangle), and the regular monomer lattice (filled diamonds). Also the CPA values calculated by Bergqvist *et al.* [26] (open squares) and Sato *et al.* [16] (open circles) are given for comparison. The lines are only to guide the eye.

the exchange coefficients correctly depend only on geometry, not on temperature or concentration.

First we briefly glance at percolation threshold Mn concentrations at which a percolation network of cluster pairs with $J_{n_i n_j} > 0$ meV is formed. The percolation thresholds for the random distribution and the thermal equilibrium distribution at 1000 K are only $[Mn] \approx 0.01$ and 0.03 , respectively. The Curie temperatures are estimated using the classical Hamiltonian of Eq. (2.12). Monte Carlo simulations are carried out in two alternating stages keeping the atomic configuration fixed. The Wolff algorithm [71] is used to sample the classical cluster-spins \vec{S}_i and the Metropolis algorithm [70] to sample the classical spin vectors \vec{S}_{ik} of the individual Mn atoms inside each cluster (i denotes the cluster and k its internal degree of freedom). Finite size effects are taken into account using Binder's cumulant method [84]. Mn distributions are generated such that they have the same cluster portions as in Fig. 4.1 in the MC cells consisting of about 55300–187000 atoms. Each simulation is replicated 20–50 times which gives T_C with an accuracy of about 3 K.

§4.2. Band structure and magnetic properties

The T_C s for the random distribution and the thermal equilibrium distribution at 1000 K are given in Fig. 4.4 (filled squares and circles, respectively). T_C depends on the Mn concentration [Mn] linearly. Our approach using ten slowly decaying $J_{n_i n_j}$ s leads to higher T_C s than that using the more rapidly decaying exchange constant obtained from the coherent potential approximation (CPA) (compare filled squares with the open squares and circles from Refs [16, 26] in Fig. 4.4). This difference is due to different treatments of microscopic interactions in our and in the CPA calculations. T_C for the random distribution is seen to exceed the room temperature at the Mn concentration of about 13.5 %. However, in thermal equilibrium at 1000 K, where significant clustering has taken place (compare the narrow right columns with the wide left ones in Fig. 4.1) we see a large drop in T_C which is directly related to clustering. To compare the Monte Carlo method against molecular field theory (§4.2.1) T_C s are also calculated for regular monomer and monomer-dimer lattices. These values are around 10-20 % higher than the T_C s for the random distribution (compare filled diamonds and triangle with the filled squares in Fig. 4.4). The high value of 514 K obtained for the regular monomer-dimer lattice at [Mn]= 0.08 in §4.2.1 has lowered drastically to the value of 187 K (filled triangle in Fig. 4.4) which is due to the inclusion of magnetic fluctuations and intra-cluster energies E_{n_i} in the present calculations. A similar large drop in T_C for (Ga,Cr)N (from 600 to less than 50 K) is found in Ref. [27].

Clustering reduces T_C for two principal reasons. First, clustering leads to an overall increase in inter-cluster separations and simultaneously decreases the number of clusters which apparently has a tendency to decrease T_C . Second, the microscopic inter-cluster exchange coefficients $J_{n_i n_j}$ depend sensitively on the cluster size with a net effect of reducing T_C . This can be seen by comparing the $J_{n_i n_j}$ s in Fig. 4.3. It is immediately clear that all $J_{n_i 4}$ s with a tetramer as a partner are significantly weaker than the corresponding other $J_{n_i n_j}$ s: J_{14} is weaker than J_{12} and J_{13} ; J_{24} is weaker than J_{22} and J_{23} ; J_{44} is weaker than J_{34} that is weaker than J_{33} . Thus, when the portion of tetramers in thermal equilibrium at 1000 K grows up to 20-40 % (depending on x , Fig. 4.1) it is natural that the T_C values undergo the dramatic drop shown in Fig. 4.4 (compare the filled circles with the filled squares).

Summary and outlook

Diluted magnetic semiconductors are promising candidates for spintronics materials, as they naturally overcome the material incompatibilities in metal-semiconductor interfaces. Of particular interest are the III-V based semiconductor materials made magnetic by inclusion of Mn (or some other suitable transition metal) that can easily be integrated in the existing III-V semiconductor technologies. In order to exploit the possibilities of this new family of materials it is crucial to understand the fundamental mechanisms behind ferromagnetism in semiconductor based materials. (Ga,Mn)As and (Ga,Mn)N are considered as important prototype materials because of their relatively high Curie temperatures T_C , and further these materials provide us with a good testing ground in the quest for new, similar materials with optimized properties.

In this thesis both (Ga,Mn)As and (Ga,Mn)N are studied theoretically starting from quantum mechanical interactions, and reaching to macroscopic properties. For both materials we find that the key element in understanding the ferromagnetism lies in understanding the atomic clustered structures and the corresponding quantum mechanical interactions. The most important findings for both materials are summarized below.

§5.1 (Ga,Mn)As

In Publications I–IV we show that the lowest energy microstructure of (Ga,Mn)As consists of Mn clusters, where the Mn atoms occupy nearest neighbor Ga sites. In Publication I we show that Mn dimers localize holes, which reduces the *effective* hole concentrations, and consequently also the hole mediated ferromagnetism gets weakened. The findings in Publication I are then generalized for larger clusters in Publications III and IV, confirming that the macroscopic magnetic properties will be determined by inter-cluster interactions instead of interactions between the individual Mn atoms. Finally in Publication V we discover the dynamic process—the vacancy mediated diffusion of Mn—which leads to clustering during growth and thermal annealing. The Curie temperatures and their long-term annealing decrease calculated based on the realistic cluster distributions are in close agreement with experimental results.

The Curie temperatures for (Ga,Mn)As are estimated only using the Weiss molecular field theory, which is known to overestimate T_C . Furthermore, known compensators such as As antisites and interstitial Mn are not included, as only idealized samples are investigated. A more quantitative description of the true experimental samples could be obtained by inclusion of further defects and using Monte Carlo methods to estimate T_C .

§5.2 (Ga,Mn)N

In Publications VI–VII we show that also in (Ga,Mn)N the lowest energy microstructure consists of substitutional Mn clusters. In (Ga,Mn)N the band splitting tendency is similar as in (Ga,Mn)As, but may lead to an *increased delocalization* for the Mn induced hole states, in particular for the Mn dimer, as shown in Publication VI. Within the Weiss molecular field theory the dimer formation leads to an increase in Curie temperature (Publication VI) due to the increased delocalization, but due to changes in $p-d$ hybridization the formation of tetramers dramatically reduces T_C . In Publication VII more sophisticated Monte

§5.2. $(Ga,Mn)N$

Carlo methods are used, showing that clustering effectively reduces T_C .

In Publications VI–VII only microscopic structures corresponding to random substitution and thermal equilibrium at 1000 K are considered. In order to quantitatively describe the experimental samples kinetic considerations should be taken into account. The more realistic microstructures can be obtained straightforwardly by calculation of migration barriers followed with kinetic Monte Carlo simulations, as done for $(Ga,Mn)As$ in Publication V.

Bibliography

[I–VII] Publications I–VII are listed on page ix.

- [1] H. Munekata, H. Ohno, S. von Molmar, Armin Segmüller, L. L. Chang, and L. Esaki, *Diluted Magnetic III-V Semiconductors*, Phys. Rev. Lett. **63**, 1849 (1989).
- [2] H. Ohno, *Making Nonmagnetic Semiconductors Ferromagnetic*, Science **281**, 951 (1998).
- [3] H. Akinaga and H. Ohno, *Semiconductor Spintronics*, IEEE Transactions on Nanotechnology **1**, 19 (2002).
- [4] T. Dietl, H. Ohno, F. Matsukura, J. Cibert, and D. Ferrand, *Zener Model Description of Ferromagnetism in Zinc-Blende Magnetic Semiconductors*, Science **287**, 1019 (2000).
- [5] T. Dietl, H. Ohno, and F. Matsukura, *Hole-mediated ferromagnetism in tetrahedrally coordinated semiconductors*, Phys. Rev. B **63**, 195295 (2001).
- [6] J. König, J. Schliemann, T. Jungwirth, and A. H. MacDonald, *Ferromagnetism in (III,Mn)V Semiconductors*, in Electronic Structure and Magnetism of Complex Materials, Eds. D. Singh and D. A. Papaconstantopoulos (Springer Verlag, Berlin 2002).
- [7] T. Jungwirth, J. Sinova, J. Mašek, J. Kučera, and A. H. MacDonald, *Theory of ferromagnetic III-V semiconductors*, submitted to Rev. Mod. Phys. (2005).
- [8] H. Akai, *Ferromagnetism and Its Stability in the Diluted Magnetic Semiconductor (In,Mn)As*, Phys. Rev. Lett. **81**, 3002 (1998).
- [9] M. Shirai, *Electronic and magnetic properties of 3d transition-metal-doped GaAs*, Physica E **10**, 143 (2001).
- [10] P. Mahadevan and A. Zunger, *First principles investigation of the assumptions underlying model-Hamiltonian approaches to*

Bibliography

- ferromagnetism of 3d impurities in III-V semiconductors*, Phys. Rev. B **69**, 115211 (2004).
- [11] K. Sato and H. Katayama-Yoshida, *Material Design of GaN-Based Ferromagnetic Diluted Magnetic Semiconductor*, Jpn. J. Appl. Phys. **40**, L485 (2001).
- [12] K. Sato and H. Katayama-Yoshida, *First principles materials design for semiconductor spintronics*, Semicond. Sci. Technol. **17**, 367 (2002).
- [13] S. Mirbt, B. Sanyala, and P. Mohn, *Magnetic properties of 3d impurities substituted in GaAs*, J. Phys.: Condens. Matter **14**, 3295 (2002).
- [14] K. Sato, P. H. Dederichs, and H. Katayama-Yoshida, *Curie temperatures of III-V diluted magnetic semiconductors calculated from first principles*, Europhys. Lett. **61**, 403 (2003).
- [15] K. Sato, P. H. Dederichs, H. Katayama-Yoshida, and J. Kudrnovský, *Magnetic impurities and materials design for semiconductor spintronics*, Physica B **340-342**, 863 (2003).
- [16] K. Sato, P. H. Dederichs, H. Katayama-Yoshida, and J. Kudrnovský, *Exchange interactions in diluted magnetic semiconductors*, J. Phys.: Condens. Matter **16**, S5491 (2004).
- [17] J. Kudrnovský, I. Turek, V. Drchal, F. Máca, J. Mašek, P. Weinberger, and P. Bruno, *Ab Initio Study of Curie temperatures of Diluted Magnetic Semiconductors*, J. Supercond. **16**, 119 (2003).
- [18] J. Kudrnovský, I. Turek, V. Drchal, F. Máca, P. Weinberger, and P. Bruno, *Exchange interactions in III-V and group-IV diluted magnetic semiconductors*, Phys. Rev. B **69**, 115208 (2004).
- [19] T. C. Schulthess, W. M. Temmermann, Z. Szotek, W. H. Butler, and G. M. Stocks, *Electronic structure and exchange coupling of Mn impurities in III-V semiconductors*, Nat. Mater. **4**, 838 (2005).
- [20] M. Berciu and R. N. Bhatt, *Effects of Disorder on Ferromagnetism in Diluted Magnetic Semiconductors*, Phys. Rev. Lett. **87**, 107203 (2001).
- [21] R. N. Bhatt, M. Berciu, M. P. Kennett, and X. Wan, *Diluted Magnetic Semiconductors in the Low Carrier Density Regime*, J. Supercond. **15**, 71 (2002).
- [22] A. Kaminski and S. Das Sarma, *Polaron Percolation in Diluted Magnetic Semiconductors*, Phys. Rev. Lett. **88**, 247202 (2002).

Bibliography

- [23] A. Kaminski and S. Das Sarma, *Magnetic and transport percolation in diluted magnetic semiconductors*, Phys. Rev. B **68**, 235210 (2003); cond-mat/0307294 (extended version, unpublished).
- [24] K. Sato, W. Schweika, P. H. Dederichs, and H. Katayama-Yoshida, *Low temperature ferromagnetism in (Ga,Mn)N: Ab initio calculations*, Phys. Rev. B **70**, 201202(R) (2004).
- [25] K. Sato, P. H. Dederichs, and H. Katayama-Yoshida, *Is High T_C Possible in (Ga,Mn)N: Monte Carlo Simulation vs. Mean Field Approximation*, J. Supercond. **18**, 33 (2005).
- [26] L. Bergqvist, O. Eriksson, J. Kudrnovský, V. Drchal, P. Korzhavyi, and I. Turek, *Magnetic Percolation in Diluted Magnetic Semiconductors*, Phys. Rev. Lett. **93**, 137202 (2004).
- [27] J. L. Xu, M. van Schilfhaarde, and G. D. Samolyuk, *Role of Disorder in Mn:GaAs, Cr:GaAs, and Cr:GaN*, Phys. Rev. Lett. **94**, 097201 (2005).
- [28] M. van Schilfhaarde and O. N. Mryasov, *Anomalous exchange interactions in III-V dilute magnetic semiconductors*, Phys. Rev. B **63**, 233205 (2001).
- [29] L. M. Sandratskii and P. Bruno, *The influence of clustering of Mn impurities on the magnetic properties of (Ga,Mn)As*, J. Phys.: Condens. Matter **16**, L523 (2004).
- [30] L. M. Sandratskii, P. Bruno, and S. Mirbt, *Effect of the Mn clustering in (Ga,Mn)N on the magnetic transition temperatures*, Phys. Rev. B **71**, 045210 (2005).
- [31] R. A. de Groot, F. M. Mueller, P. G. van Engen, and K. H. J. Buschow, *New Class of Materials: Half-Metallic Ferromagnets*, Phys. Rev. Lett. **50**, 2024 (1983).
- [32] W. E. Pickett and J. S. Moodera, *Half-metallic magnets*, Physics Today **54**, 39 (2001).
- [33] K. W. Edmonds, P. Bogusławski, K. Y. Wang, R. P. Champion, S. N. Novikov, N. R. S. Farley, B. L. Gallagher, C. T. Foxon, M. Sawicki, T. Dietl, M. Buongiorno Nardelli, and J. Bernholc, *Mn Interstitial Diffusion in (Ga,Mn)As*, Phys. Rev. Lett. **92**, 037201 (2004).
- [34] K. Y. Wang, R. P. Champion, K. W. Edmonds, M. Sawicki, T. Dietl, C. T. Foxon, and B. L. Gallagher, *Magnetism in (Ga,Mn)As*

Bibliography

- Thin Films With T_C Up To 173 K*, AIP Conference Proceedings **772**, 333 (2005); cond-mat/0411475.
- [35] S. J. Pearton, C. R. Abernathy, G. T. Thaler, R. M. Frazier, D. P. Norton, F. Ren, Y. D. Park, J. M. Zavada, I. A. Buyanova, W. M. Chen, and A. F. Hebard, *Wide bandgap GaN-based semiconductor for spintronics*, J. Phys.: Condens. Matter **16**, R209 (2004).
- [36] H. Ohno, A. Shen, F. Matsukura, A. Oiwa, A. Endo, S. Katsumoto, and Y. Iye, *(Ga,Mn)As: A new diluted magnetic semiconductor based on GaAs*, Appl. Phys. Lett. **69**, 363 (1996).
- [37] A. Shen, H. Ohno, F. Matsukura, Y. Sugawara, N. Akiba, T. Kuroiwa, A. Oiwa, A. Endo, S. Katsumoto, and Y. Iye, *Epitaxy of (Ga,Mn)As, a new diluted magnetic semiconductor based on GaAs*, J. Cryst. Growth **175-176**, 1069 (1997).
- [38] F. Matsukura, A. Oiwa, A. Shen, Y. Sugawara, N. Akiba, T. Kuroiwa, H. Ohno, A. Endo, S. Katsumoto, and Y. Iye, *Growth and properties of (Ga,Mn)As: A new III-V diluted magnetic semiconductor*, Appl. Surf. Sci. **113-114**, 178 (1997).
- [39] H. Ohno, *Properties of ferromagnetic III-V semiconductors*, J. Magn. Magn. Mater. **200**, 110 (1999).
- [40] S. J. Potashnik, K. C. Ku, S. H. Chun, J. J. Berry, N. Samarth, and P. Schiffer, *Effects of annealing time on defect-controlled ferromagnetism in $(Ga_{1-x},Mn_x)As$* , Appl. Phys. Lett. **79**, 1495 (2001).
- [41] M. Adell, J. Kanski, L. Ilver, J. Sadowski, V. Stanciu, and P. Svedlindh, *Comment on "Mn Interstitial Diffusion in $(Ga,Mn)As$ "*, Phys. Rev. Lett. **94**, 139701 (2005)
- [42] V. Stanciu, O. Wilhelmsson, U. Bexell, M. Adell, J. Sadowski, J. Kanski, P. Warnicke, and P. Svedlindh, *Influence of annealing parameters on the ferromagnetic properties of optimally passivated $(Ga,Mn)As$ epilayers*, Phys. Rev. B, 125324 (2005).
- [43] S. Sanvito, P. Ordejón, and N. A. Hill, *First-principles study of the origin and nature of ferromagnetism in $Ga_{1-x}Mn_xAs$* , Phys. Rev. B **63**, 165206 (2001).
- [44] E. Kulatov, H. Nakayama, H. Mariette, H. Ohta, and Yu. A. Uspenski, *Electronic structure, magnetic ordering, and optical properties of GaN and GaAs doped with Mn*, Phys. Rev. B **045203** (2002).

Bibliography

- [45] L. Bergqvist, P. A. Korzhavyi, B. Sanyal, S. Mirbt, I. A. Abrikosov, L. Nordström, E. A. Smirnova, P. Mohn, P. Svedlindh, and O. Eriksson, *Magnetic and electronic structure of $(Ga_{1-x},Mn_x)As$* , Phys. Rev. B **67**, 205201 (2003).
- [46] L. M. Sandratskii, P. Bruno, and J. Kudrnovský, *On-site Coulomb interaction and the magnetism of $(Ga,Mn)N$ and $(Ga,Mn)As$* , Phys. Rev. B **69**, 195203 (2004).
- [47] M. Wierzbowska, D. Sánchez-Portal, and Stefano Sanvito *Different origins of the ferromagnetic order in $(Ga,Mn)As$ and $(Ga,Mn)N$* , Phys. Rev. B **70**, 235209 (2004).
- [48] R. Giraud, S. Kuroda, S. Marcet, E. Bellet-Amalric, X. Biquard, B. Barbara, D. Fruchart, D. Ferrand, J. Cibert, and H. Mariette, *Ferromagnetic $Ga_{1-x}Mn_xN$ epilayers vs. antiferromagnetic $GaMn_3N$ clusters*, Europhys. Lett. **65**, 552 (2004).
- [49] S. Dhar, O. Brandt, A. Trampert, L. Därewitz, K. J. Friedland, K. H. Ploog, J. Keller, B. Beschoten, and G. Güntherodt, *Origin of high-temperature ferromagnetism in $(Ga,Mn)N$ layers grown on $4H-SiC(0001)$ by reactive molecular-beam epitaxy*, Appl. Phys. Lett. **82**, 2077 (2003).
- [50] N. Theodoropoulou, A. F. Hebard, M. E. Overberg, C. R. Abernathy, S. J. Pearton, S. N. G. Chu, and R. G. Wilson, *Magnetic and structural properties of Mn implanted GaN*, Appl. Phys. Lett. **79**, 3475 (2001).
- [51] M. L. Reed, N. A. El-Masry, H. H. Stadelmaier, M. K. Ritums, M. J. Reed, C. A. Parker, J. C. Roberts, and S. M. Bedair, *Room temperature ferromagnetic properties of $(Ga,Mn)N$* , Appl. Phys. Lett. **79**, 3473 (2001).
- [52] M. E. Overberg, C. R. Abernathy, S. J. Pearton, N. A. Theodoropoulou, K. T. McCarthy, and A. F. Hebard, *Indication of ferromagnetism in molecular-beam-epitaxy-derived N-type GaMnN*, Appl. Phys. Lett. **79**, 1312 (2001).
- [53] M. C. Park, K. S. Huh, J. M. Myoung, J. M. Lee, J. Y. Chang, K. I. Lee, S. H. Han, and W. Y. Lee, *Room temperature ferromagnetic $(Ga,Mn)N$ epitaxial films with low Mn concentration grown by plasma-enhanced molecular beam epitaxy*, Solid State Commun. **124**, 11 (2002).
- [54] S. Sonoda, S. Shimizu, T. Sasaki, Y. Yamamoto, and H. Hori, *Molecular beam epitaxy of wurtzite $(Ga,Mn)N$ films on sap-*

Bibliography

- phire(0001) showing the ferromagnetic behaviour at room temperature*, J. Cryst. Growth **237-239**, 1358 (2002).
- [55] T. Sasaki, S. Sonoda, Y. Yamamoto, K. Suga, S. Shimizu, K. Kindo, and H. Hori, *Magnetic and transport characteristics on high Curie temperature ferromagnet Mn-doped GaN*, J. Appl. Phys. **91**, 7911 (2002).
- [56] G. T. Thaler, M. E. Overberg, B. Gila, R. Frazier, C. R. Abernathy, S. J. Pearton, J. S. Lee, S. Y. Yee, Y. D. Park, Z. G. Khim, J. Kim, and F. Ren, *Magnetic properties of n-GaMnN thin films*, Appl. Phys. Lett. **80**, 3964 (2002).
- [57] P. Langevin, *Magnétisme et théorie des électrons*, Ann. Chim. Phys., 8° série **5**, 70 (1905).
- [58] P. Weiss, *L'hypothèse du champ moléculaire et la propriété ferromagnétique*, J. de Phys., 4° série **6**, 661 (1907).
- [59] W. Heisenberg, *Zur Theorie des Ferromagnetismus*, Z. Phys. **49**, 619 (1928).
- [60] P. Hohenberg and W. Kohn, *Inhomogeneous Electron Gas*, Phys. Rev. **136**, B864 (1964).
- [61] P. Blochl, *Projector augmented-wave method*, Phys. Rev. B **50**, 17953 (1994).
- [62] G. Kresse and J. Furthmüller, *Efficient iterative schemes for ab initio total-energy calculations using a plane wave basis set*, Phys. Rev. B **54**, 11169 (1996); *ibid.*, *VASP the Guide* (Vienna University of Technology 1999) [<http://tph.tuwien.ac.at/~vasp/guide/vasp.html>].
- [63] J. C. Slater, *The Self-consistent Field for Molecules and Solids Volume 4: Quantum Theory of Molecules and Solids* (McGraw-Hill, 1974).
- [64] S. Chikazumi, *Physics of Magnetism*, (John Wiley & Sons, 1964).
- [65] N. W. Ashcroft and N. D. Mermin, *Solid State Physics*, (Holt, Rinehart and Winston, 1976).
- [66] A. I. Liechtenstein, M. I. Katsnelson, V. P. Antropov, and V. A. Gubanov, *Local spin density functional approach to the theory of exchange interactions in ferromagnetic metals and alloys*, J. Magn. Magn. Mater. **67**, 65 (1987).

Bibliography

- [67] Ph. Kurz, G. Bihlmayer, and S. Blügel, *Magnetism and electronic structure of hcp Gd and the Gd(0001) surface*, J. Phys.:Condens. Matter **14**, 6353 (2002).
- [68] I. Turek, J. Kudrnovský, G. Bihlmayer, and S. Blügel, *Ab initio theory of exchange interactions and the Curie temperature of bulk Gd*, J. Phys.:Condens. Matter **15**, 2771 (2003).
- [69] K. Sato, H. Katayama-Yoshida, and P. H. Dederichs, *Dilute Magnetic Semiconductors*, Ψ_k Newsletter **70**, 93 (2005).
- [70] N. Metropolis, A. W. Rosenbluth, M. N. Rosenbluth, A. H. Teller, and E. Teller, *Equation of State Calculations by Fast Computing Machines*, J. Chem. Phys. **21**, 1087 (1953)
- [71] U. Wolff, *Collective Monte Carlo Updating for Spin Systems*, Phys. Rev. Lett. **62**, 361 (1989).
- [72] W. Kohn and L. J. Sham, *Self-Consistent Equations Including Exchange and Correlation Effects*, Phys. Rev. **140**, A1133 (1965).
- [73] O. Gunnarson and B. I. Lundqvist, *Exchange and correlation in atoms, molecules and solids by the spin-density-functional formalism*, Phys. Rev. B **13**, 4274 (1976).
- [74] J. P. Perdew and A. Zunger, *Self-interaction correction to density-functional approximations for many-electron systems*, Phys. Rev. B **23**, 5048 (1981).
- [75] J. P. Perdew, J. A. Chevary, S. H. Vosko, K. A. Jackson, M. R. Pederson, D. J. Singh, and C. Fiolhais, *Atoms, molecules, solids, and surfaces: Applications of the generalized gradient approximation for exchange and correlation*, Phys. Rev. B **46**, 6671 (1992).
- [76] V. I. Anisimov, J. Zaanen, and O. K. Andersen, *Band theory and Mott insulators: Hubbard U instead of Stoner I*, Phys. Rev. B **44**, 943 (1991).
- [77] S. L. Dudarev, G. A. Botton, S. Y. Savrasov, C. J. Humphreys, and A. P. Sutton *Electron-energy-loss spectra and the structural stability of nickel oxide: An LSDA+U study*, Phys. Rev. B **57**, 1505 (1998).
- [78] F. Tuomisto, K. Pennanen, K. Saarinen, and J. Sadowski, *Ga sublattice defects in (Ga,Mn)As: thermodynamic and kinetic trends*, Phys. Rev. Lett. **93**, 055505 (2004).

Bibliography

- [79] M. Bockstedte and M. Scheffler, *Theory of self-diffusion in GaAs*, Z. Phys. Chem. **200**, 195 (1997).
- [80] J-L. Rouviere, Y. Kim, J. Cunningham, J. A. Rentschler, A. Bourret, and A. Ourmazd, *Measuring Properties of Point Defects by Electron Microscopy: The Ga Vacancy in GaAs*, Phys. Rev. Lett. **68**, 2798 (1992).
- [81] L. Wang, L. Hsu, E. E. Haller, J. W. Erickson, A. Fischer, K. Eberl, and M. Cardona, *Ga Self-Diffusion in GaAs Isotope Heterostructures*, Phys. Rev. Lett. **76**, 2342 (1996).
- [82] H. Bracht, M. Norseng, E. E. Haller, K. Eberl, and M. Cardona, *Enhanced and retarded Ga self-diffusion in Si and Be doped GaAs isotope heterostructures*, Solid State Commun. **112**, 301 (1999).
- [83] M. G. Ganchenkova, V. A. Borodin, and R. M. Nieminen, *Annealing of vacancy complexes in P-doped silicon*, Nucl. Inst. Meth. Phys. Res. B **228**, 218 (2005).
- [84] K. Binder, *Critical Properties from Monte Carlo Coarse Graining and Renormalization*, Phys. Rev. Lett. **47**, 693 (1981).